5-2018

Behavior Coding Strategies: Population Coupling and the Functional Role of Excitatory/Inhibitory Balance in Primary Motor Cortex

Patrick Aaron Kells
University of Arkansas, Fayetteville

Behavior Coding Strategies: Population Coupling and the Functional Role of Excitatory/Inhibitory Balance in Primary Motor Cortex

A dissertation submitted in partial fulfillment
of the requirements for the degree of
Doctor of Philosophy in Physics

by

Patrick Kells
University of Central Arkansas
Bachelor of Science in Physics, 2009

May 2018
University of Arkansas

This dissertation is approved for recommendation to the Graduate Council.

_____
Woodrow Shew, Ph.D.
Dissertation Director

_____
Paul Thibado, Ph.D.
Committee Member

_____
Nathan Parks, Ph.D.
Committee Member

Abstract

The complexities of an organism's experience of- and interaction with the world are emergent phenomena produced by large populations of neurons within the cerebral cortex and other brain regions. The network dynamics of these populations have been shown to be sometimes synchronous, with many neurons firing together, and sometimes asynchronous, with neurons firing more independently, leading to a decades-old debate within the neuroscience community. This discrepancy comes from viewing the system at two different scales; at the single cell level, the spiking activity of two neurons within cortex tend to be rather independent, but when the average activity of a global population is measured (e.g. during EEG, LFP measurements), large scale oscillations are typically observed. Both modes confer certain benefits and drawbacks in regard to information processing. Synchronous networks display more robust signal propagation at the expense of lower information capacity and higher signal-to-noise while more asynchronous networks exhibit higher information capacity but lack strong signal throughput. Do either of these scenarios prevail within motor cortex or do the two regimes work simultaneously to produce behavior? Here we measure neuron-to-population and neuron-to-body coupling of neurons within primary motor cortex of awake, freely behaving rats. We found that neurons with high and low population coupling coexist within cortex and population coupling was tunable via modulation of inhibitory signaling. Thus, our results show that both high and low synchrony neurons coexist. We also found that neurons with high and low population coupling serve different functional roles; neurons with low values of population coupling were more strongly coupled to the activity of the body, while neurons which were more engaged with the population tended to be less responsible in commanding body movement. These findings suggest a possible optimization strategy- the neurons that are most responsible for body movements are balanced between synchronous and asynchronous network activity, making a compromise between the various benefits and disadvantages of either extreme synchrony or extreme asynchrony.

Acknowledgments

First, I would like to thank all past and present members of my committee for their encouragement and constructive criticisms throughout my graduate work. Thanks to our postdoc, Dr. Shree Hari Gautam. Without his surgical expertise, this research would not have been possible. I would like to thank my mother for her strength and grace. Without whose guidance and support I would not be where I am today. A special thanks to my best friend and accomplice of the past seven years, Sean Nomoto, with whom I could always be myself fully, without fear of judgement. To my dog, Hank for showing me the importance of patience and structure, and the joy found in service. To my friends Josh Davis, Nick Wolfe, and Reece Davis for relentlessly modeling the passionate and uncompromising approach to life. To my labmate, Jingwen Li for her unparalleled positivity and contagious smile. To the students in my physics labs who made teaching the best part of graduate school. And to all my friends and coworkers at the Community Creative Center who provided relief from the various pressures of life. Finally, I would like to offer my sincerest thanks to my advisor, Dr. Woodrow Shew, who introduced me to the art of objective experimental design and data analysis techniques. And whose utmost patience, kindness, and optimism showed me how to properly deal with the inevitable blunders of collaborative research. I could not have asked for a better mentor and teacher.

Dedication

This dissertation is dedicated to our failures, the seeds of growth.

Table of Contents

Introduction

The coordinated interactions between an organism and its external environment depend on the conversion of raw sensory input to internal planning, and eventually motor output via a group of interconnected cells (neurons) known collectively as the nervous system. The human nervous system with its hundred billion neurons and hundred trillion connections (axons and dendrites), at first glance, seems indistinguishable from a tangled mess. However, upon closer inspection, a highly organized network structure emerges with complexity which rivals that of any systems found in nature.

This complexity emerges from interactions between various components across multiple scales (Kandel et al. 2014) (figure 1). On a more global scale, regions of the brain (cortex, thalamus, hippocampus, etc.) communicate via large bundles of axons which transmit information in the form of electrical pulses, or action potentials, from one region to another. Focusing on one of these larger areas, for instance the cerebral cortex, reveals smaller scale function-specific circuits (visual, motor, auditory, etc.) which interact through certain structures and pathways to produce a more unified experience (Andersen 1997; Illing 1996). Zooming in further reveals these circuits are composed of populations of individual neurons which interact to produce- and code for information specific to a particular region (e.g. information pertaining to the planning and execution of reaching movements occurs primarily in motor cortex). Most of these individual neurons can be classified, in the broadest sense, as either excitatory or inhibitory. This classification is dictated by the effect a neuron has on other, downstream neurons within the network, more specifically, whether its signals increase (excitatory) or decrease (inhibitory) the membrane potential (voltage difference across a neuron's cell wall) of downstream neurons.

Neurons integrate incoming action potentials over both space and time via specialized junctions (synapses) located along the cell body (soma) and dendrites. If a downstream neuron

receives enough excitatory input in a short enough time, the membrane potential will cross a neuron-specific threshold value at which point the neuron will send an action potential out to its downstream neurons. On the other hand, because inhibitory signals drive the membrane potential away from this threshold value, these threshold crossings can be repressed if enough inhibitory signals are present. In this way, these two types of neurons can be said to be in a competition.

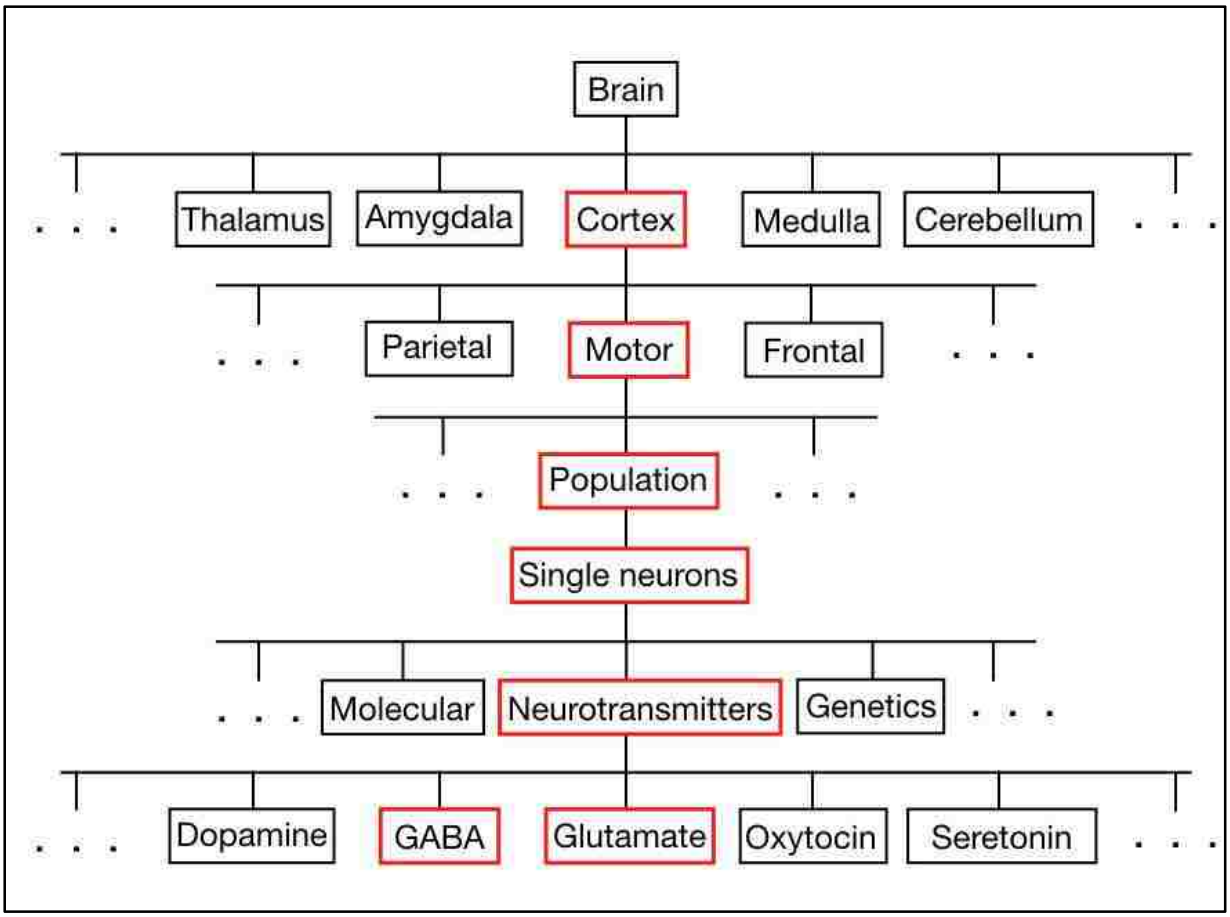

Figure 1 - Regions of interest within the brain. This study focuses on the areas outlined in red, namely population dynamics in motor cortex using single neuron spiking activity and how the balance of excitatory and inhibitory input (controlled by glutamate and GABA neurotransmitters respectively) affects those dynamics.

The balance of excitation and inhibition (E/I) within a natural, healthy brain is poised at somewhat of a 'Goldilocks' ratio. If the network contains too many excitatory neurons, signals become overly amplified and large-scale oscillatory fluctuations dominate which can lead to certain neurological disorders (autism spectrum disorder, epilepsy, etc.) (Buckley and Holmes

2016). On the other hand, if too much inhibition is present, signals die out prior to reaching target neurons and, in extreme circumstances, the activity of the network can become silenced (Sitdikova et al. 2014). However, if the ratio of excitation to inhibition is 'just right', signals can propagate through the network without runaway excitation. Previous work has shown that many of the emergent phenomena of neural networks (information capacity and transmission, dynamic range, etc.) are maximized when E/I is properly balanced (Shew et al. 2011; Gautam et al. 2015). Herein, we attempt to closely examine behavior coding strategies at the level of individual neurons in primary motor cortex and how this balance of excitation and inhibition affects said strategies.

In a broad sense, the organization of- and method by which information is processed in cortex is a controversial subject which has been debated for decades. Some of this debate comes from viewing the system at two different scales. At the macroscopic level, the collective activity, averaged over many neurons of the cortex seems highly synchronous (Gray and Singer 1989; Womelsdorf et al. 2007; Canolty et al. 2010; Markopoulos et al. 2012). However, when comparing the cortical activity of any two single neurons within the same population, the neurons often fire rather independently of each other, suggesting that the network is in a more disordered, asynchronous state (Gawne and Richmond 1993; Renart et al. 2010; Ecker et al. 2010). Both the asynchronous scenario and the synchronous scenario have potential benefits and drawbacks in regard to information processing.

The most obvious benefit of synchronous networks is robust signal throughput (Salinas and Sejnowski 2001; Womelsdorf et al. 2007; Zohary, Shadlen, and Newsome 1994; Riehle et al. 2009) through utillizing strength in numbers (i.e. for a given stimulus, the larger the total network fluctuations the greater the probability a signal will reach its respective target neurons). Second, fluctuations of single neuron firing times around large-scale synchronous activity could represent a temporal coding strategy for sensory stimulus (Uhlhaas et al. 2009; O'Keefe and Recce 1993). Finally, global synchrony across large-scale circuits within cortex could account

for the fluidity of composite sensations within consciousness ultimately leading to a single, unified experience (Uhlhaas et al. 2009; Stein, Stanford, and Rowland 2009). One major drawback to a highly synchronous network is that noise signals would also propagate more robustly, giving rise to lower signal-to-noise ratios (Cohen and Kohn 2011; Averbeck, Latham, and Pouget 2006). Another potential drawback of a synchronous network is that many neurons are used to code the same information, which could limit how much information is encoded.

On the other hand, a more asynchronous network, while not benefiting from strength in numbers, can generate a bigger repertoire of different firing patterns. This large repertoire of states equates to a higher network information capacity (Rolls, Treves, and Tovee 1997; Shew et al. 2011; Schneidman, Bialek, and Berry 2003) which translates to a wider range of possible perceived sensations (in sensory cortex) or motor actions (in motor cortex) for an organism.

How can we reconcile these two discrepant points of view? One possibility is that the synchronous and asynchronous coding strategies operate in tandem. This could be the case if a minority of neurons fire together in synchrony. Then the average collective activity could still appear to be synchronous, because the asynchronous neurons cancel each other out on average leaving only the signal of the synchronous neurons at the macroscopic scale. This scenario would also be consistent with observations that a randomly chosen pair of neurons tends to fire asynchronously (Gawne and Richmond 1993; Renart et al. 2010; Ecker et al. 2010). If this scenario is true, then we would expect to find that some small fraction of neurons is strongly coupled to the population while others are not.

Recent work (Okun et al. 2015) has shown exactly this. More specifically, by utilizing high density electrode arrays inserted into primary visual cortex in awake mice, the researchers were able to measure the spike activity of many neurons simultaneously. They found that some of these neurons were strongly coupled to the population while others were weakly coupled to the population. They also showed that neurons which are more strongly coupled to the activity of the population in which they are embedded tended to be most responsive to visual stimulus.

This high responsiveness to visual stimulus suggests that those neurons with high values of population coupling are most likely responsible for coding of visual stimulus. They were also able to determine that the population coupling strength of a neuron is relatively independent of visual stimulus, meaning that population coupling is, in large part, due to the anatomical structure of the network or cell and not an effect that varies over time, which agrees with previous findings (Pernice et al. 2011; Helias, Tetzlaff, and Diesmann 2014) that network connectivity determines the degree of synchrony throughout a network. The primary goal of the work presented in this thesis was to ask similar questions about neurons in motor cortex. Which neurons in motor cortex are strongly or weakly coupled to the population? Which are responsible for generating body movements?

Several studies have demonstrated the significance of synchronous activity between cortical neurons in motor cortex. One study (Maynard et al. 1999; Hatsopoulos et al. 1998) in particular, through a reaching task in awake macaque monkeys, found that the correlation strength between the activity of pairs of neurons in primary motor cortex (M1) were heavily dependent on reach direction. By utilizing extracellular recordings from 100-electrode arrays implanted in M1 alongside an 8-way directional reaching task, they were able to show that the direction-specific information coded within the joint activity of pairs of correlated neurons was greater than the information coded within their individual spike rates alone.

Although the importance of the joint activity between pairs of individual neurons in M1 has proven significant for the coding of behavior during task related activities, the relationship between single neurons to the larger activity of the population has not yet been closely examined in the context of spontaneous behavior. The bulk of experiments conducted in the realm of motor cortex focus primarily on task-related behavior events (Georgopoulos 1996; Murthy et al. 2013; Maynard et al. 1999). When these task-related events (often on the order of hundreds) are analyzed, the spontaneous, or ‘ongoing’ activity of the network is averaged out and so is not a topic of interest. While analysis of coding strategies for specific behaviors can

possibly help us infer more general coding strategies of cortex, in this study we attempt to determine the relationship between individual neuron-to-population and neuron-to-body coupling strengths in the context of spontaneous (both neural and behavior) activity. To do this, we apply population coupling and novel body coupling analyses to simultaneously recorded neural and behavior data in awake, freely behaving rats.

The initial motivation for this work stems from previous studies (Nelson and Valakh 2015; Fagiolini and Leblanc 2011; Buckley and Holmes 2016) on autism spectrum disorder (ASD) which suggest an imbalance in the E/I ratio. ASD individuals are often diagnosed based on certain signature behavior traits (i.e. repetitive movements, social interaction difficulties, etc.). Because a large repertoire of an ASD individual's behavior is repetitive, studying task related events for autistic individuals against control groups may not be as valuable as contrasting the spontaneous activity between these groups. Therefore, while this study mainly focuses on coding strategies within motor cortex, the results herein will hopefully lay a foundation for exposing the (still largely unknown) mechanisms of ASD and other related neurological disorders.

In this thesis, we hypothesize several important results: (1) population coupling takes on a spectrum of values within motor cortex, (2) neurons with high and low values of population coupling have separate functional roles in behavior coding, and (3) the range of neuron population coupling values and their specific roles in behavior coding depend on the balance of excitation and inhibition in cortex.

Experimental methods

Animals are shipped to the university animal care facility a minimum of two weeks prior to their chronic surgery date. They are housed in multi-occupancy cages with 3-5 animals per cage. Each cage is lined with corn husk bedding which is changed at most every other day. The animals are free-fed chow and water which are readily available through a grate located on the top portion of the cage.

Due to the nocturnal nature of the rat and the daytime hours at which we perform our experiments, the animals' day/night cycle is inverted upon delivery to the facility. This ensures proper wakefulness and exploratory behavior when animals would otherwise be resting. This procedure was observed during the initial set of animals (global inhibitory modulation experiments). However, due to an administrative change at the animal care facility, this detail was overlooked when housing animals for the local inhibitory modulation experiments, i.e. these animals were housed on a natural light cycle.

In order to become acclimatized to human touch during experiments, animals are handled 3-4 times per week leading up to surgery. These handling sessions should be brief initially (5-minute maximum) and physical contact should be kept to a minimum. Progressively, session time and physical touch should be increased at a rate which is noticeably comfortable for the animals. During these contact sessions, each animal should be trained to accept bacon-flavored (placebo) treats which, after their surgery, will administer painkillers as well as antibiotics.

During the acclimatization time period, materials for the MEA (multi-electrode array) (A8x4-2mm-200-200-413-CM32, Neuronexus) implant can be prepared. In order for the MEA to be properly grounded when inside the skull, a silver chloride (AgCl) pellet is soldered to the MEA as outlined below. Another important component of the implant is the anchor (figure 2) which stabilizes the electrodes from unwanted movements within the cortex while attached to the headstage during recordings.

The anchor which minimizes unwanted motion of the probes is machined from billet aluminum. The anchor consists of a lower piece (anchor bottom), and an upper piece (anchor top) (figure 2). These two pieces are machined such that when the electrode is attached to the headstage, the aluminum surfaces are mated together and can be properly secured with a small screw through the anchor top which screws into a threaded hole within the anchor bottom. The anchor bottom is inserted and fixed in place with dental cement alongside the probe while the anchor top is permanently fixed to the recording headstage via clear epoxy. To ensure proper fit between the anchor top and bottom during recordings, the anchor top is glued to the headstage with the anchor bottom attached. Similarly, when inserting the probe during the craniotomy, the anchor top and anchor bottom are inserted as a single piece (though only the anchor bottom is fixed with dental cement).

MEA probes are outfitted with an internal grounding mechanism. However, to ensure proper grounding throughout implant times on the order of months, probes are modified to include a small AgCl pellet which is more resilient to attacks from the animal's immune system (primarily due to its larger size). The company which supplies the probes (Neuronexus) makes a variety of styles of probe to suit many unique applications. The experiments performed here utilized the 'Gen. 3' style probe, with which a Probe Reference site (external ground) was used. In order to use the external ground, the 'Reference Jumper 2' should be disconnected (removed) and the white 'Wire 1' should be cut and removed. Finally, the AgCl pellet can be soldered to the green 'Ground' wire (figure 3).

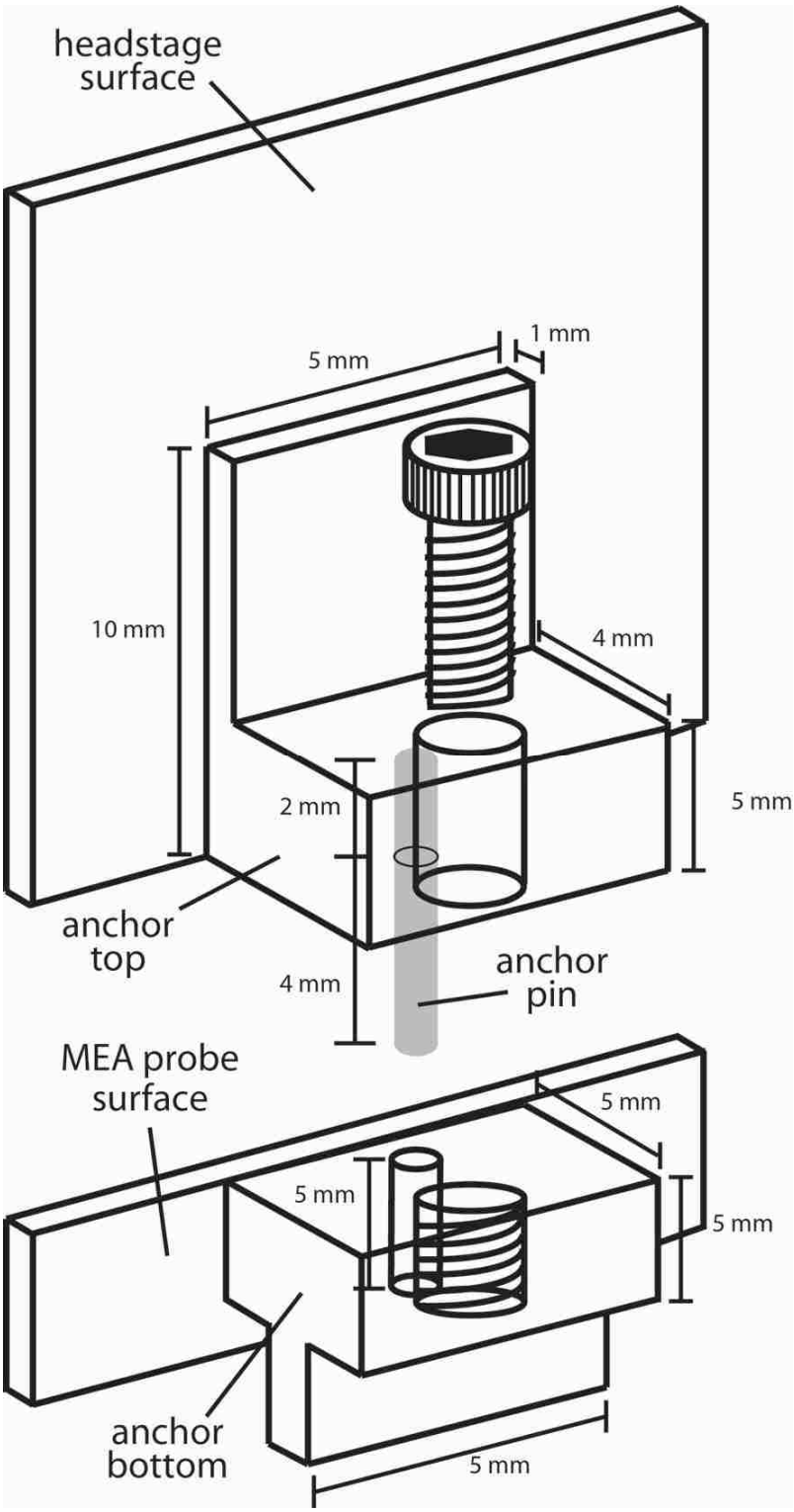

Figure 2 - MEA probe anchor attachment. Due to the size of recording electrodes, shifts in electrode positions with respect to neural tissue can cause fluctuations in recorded voltage potentials. To reduce these micro-movements an aluminum anchor is cemented alongside the MEA probe during surgery via dental cement. During recording sessions, the anchor pin (which is fixed inside the top anchor) is inserted into the bottom anchor and the surfaces are mated together with a small allen screw.

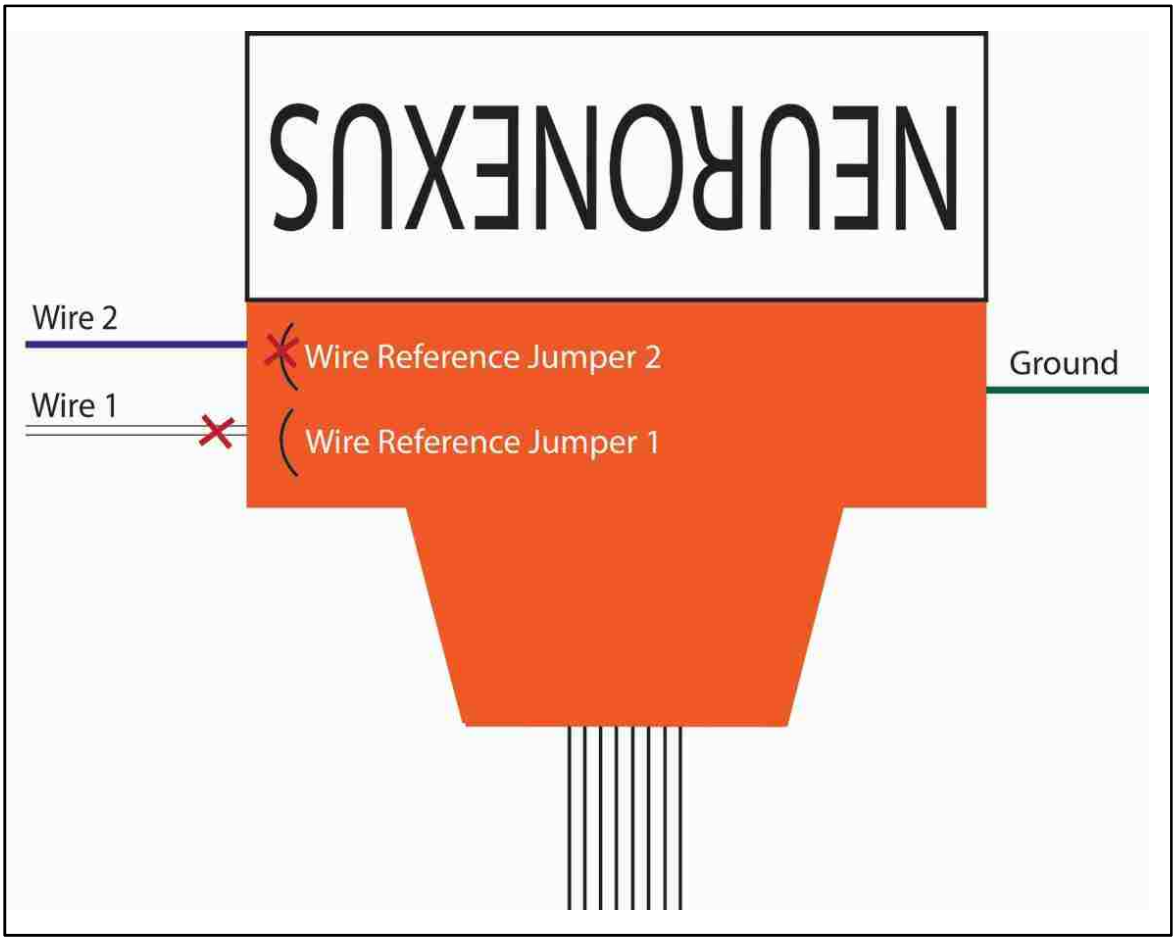

Figure 3 - Preparation of the AgCl pellet for sufficient ant resilient grounding of the MEA probe. With the probe positioned as seen above, both 'Wire Reference Jumper 2' and 'Wire 1' (white wire) should be removed from the probe (indicated with red 'x'). Finally, the green 'Ground' wire can be stripped and soldered to a new AgCl ground pellet.

On the morning of the surgery day animals are transported from CLAF to the surgery room in the physics building and left to rest until the time of surgery which typically occurs in the afternoon. This waiting period allows for any stress due to transportation to subside before the operation. It should be noted that recovery from surgery is directly related to the amount of physical and mental stress placed on the animal therefore all attempts are made to minimize any possible stressors. Upon delivery, animals are checked for proper health (physical traits such as eyes, behavior and weight) to ensure the most successful surgery possible.

Prior to handling animals for surgery, proper sterilization procedures must be performed to reduce the risk of any possible post-surgery bacterial infections. It is important that

the surgery room, equipment, as well as the surgeon are properly sterilized. Prior to sanitizing room surfaces, any possible sources of drafts should be minimized to keep future airborne deposition of bacteria as low as possible. For sterilization of the room, surfaces (workbench, countertops, flow hood, etc.) should be dusted/vacuumed and (excluding the floor) finally wiped down with alcohol, Lysol, or an equivalent disinfectant. Tools and beakers should be cleaned first with distilled water then alcohol. Tools should be placed in the Germinator to be heat treated for no less than 2 hours and allowed to cool prior to surgery. As for the surgeon, hands and arms (up to elbows) should be scrubbed with antibacterial soap for a minimum of 1 minute after which a surgical gown and sterile exam gloves should be worn throughout the remainder of the surgery.

The rat data sheet should be properly filled out which includes the animal's physical attributes, type of surgery being performed, drugs used throughout (type, dosage, and time), frequent pain reflex tests, and any special notes unique to that animal's procedure. After the above steps are completed the surgery can begin.

The anesthetic used throughout the surgery is isoflurane. For induction (putting the animal from waking into an anesthetized state) the animal is placed inside an enclosed chamber with an inlet and an outlet. During induction, the inlet is fed a 5% isoflurane concentration, which in turn flushes ambient air via the exhaust outlet which attaches to a specialized carbon filter to collect any unspent isoflurane. Once the animal is unconscious, the concentration is lowered to 3% after which the animal's breathing is monitored until a steady breathing rate of ~1-1.5 breaths/second is observed. The animal is now properly anesthetized and can be moved to the stereotaxic table for surgery.

Once placed on the stereotaxic table, the heating pad/temperature sensors should be switched on and the internal temperature probe should be coated in petroleum jelly and inserted into the animal's rectum (~2 inches deep). The protruding wire should then be taped to the animal's tail to prevent it from sliding out during surgery. Initial injections of antibiotic

(enrofloxacin, intraperitoneal) and anti-inflammatories (dexamethasone, intramuscular) are given and recorded on the data sheet. Once the temperature probe is inserted and initial injections are administered, a surgical drape is placed over the body of the animal to prevent any bacteria from the body/hair of the rat from moving up to the surgical site. The drape is placed in such a way that observations of the side/belly of the animal can be easily made as the frequency and depth of breathing are first indicators of any possible surgical abnormalities.

Head-fixing ear bars are inserted into the animal's external auditory meatus which are located ventral to the ear hole. The stage should be elevated to allow the animal to rest naturally and with no obstruction of its airway. The animal should be placed on the stage such that its ear holes are naturally aligned with the ear bars (neither a stretched or compressed neck) and measurements on the ear bars are equal once fixed (not shifted to one side of the stage).

The surgical site is shaved with clippers (hair is vacuumed away once removed) then saturated with iodine via a sterile cotton swab. Opthalmic ointment is liberally applied to the animal's eyes and should be maintained throughout the duration of the surgery to prevent drying of the eyes. After the iodine has been in place for 3-5 minutes, the excess is wiped away using a clean swab and a local anesthetic (lidocaine) is applied to the surface of, and underneath, the epidermis and allowed to sit for at least 1 minute. The initial incision should be made along the midline from the base of the skull up to a point between the eyes. It should be made in a single, fluid motion while being deep enough to penetrate the dermis but not so deep that it cuts into the tissue of the skull. If any portion of the epidermis/dermis is not fully opened, a minimal number of cuts should be made with scissors to allow for an adequate working surgical area. Using the minimum number of cuts speeds up recovery time and minimizes the surface area upon which any infections could occur.

Upon opening, the animal will bleed from the incised wound as well as small sites on the surface of the skull. Initially, pressure should be applied to the wound for a few seconds using

fresh gauze, after which time the bleeding should mostly subside. If the epidermis still shows signs of bleeding more gauze compresses can be applied. Clotting can be induced on the surface of the skull by scraping with forceps and application of pressure through cotton swabs. If any bleeding point refuses to clot, it may be cauterized but only as a last resort as the high temperature permanently kills the tissue.

As soon as all bleeding points are stopped, the surface of the skull should be saturated with fresh saline solution. This process of hydration should occur frequently enough such that the surface never becomes excessively dry (whitening of bone and blackening of any blood are the clearest indicators of dryness). Once rehydrated a very thin layer of super glue is applied to the surface of the skull using a clean cotton swab (being careful not to apply to the skin). Any excess super glue should be wiped away with second fresh swab. This thin layer of glue helps keep bleeding sites on the surface of the skull to a minimum while simultaneously reducing dehydration throughout the surgery.

In order to anchor the probe which will be inserted after the craniotomy, stainless steel screws are placed in the skull along the perimeter of the opening (figure 4). Pilot holes are drilled in 5 points (3 on the opposing side of the midline from the craniotomy window and 2 on the same side) which are spaced far enough apart to maximize coverage of the allowed surface area. Screw and ground pellet (discussed later) locations should be decided upon prior to drilling and marked with a Sharpie or some other marking scheme. Screw holes are made using a dental drill with a correspondingly sized 90° cutting tip and the stereotaxic arm. Holes should be made perpendicular to the surface of the skull which can be accomplished by setting a ~15-20° vertical angle on the stereotaxic arm. The thickness of the skull tissue varies (with more thick portions being in the posterior portion) but a depth of 1mm is a safe starting point for drill sites. While holding the head fixed via forceps firmly planted on the surface of the skull, holes are drilled completely through so screws can be inserted fully and without obstruction. The process of drilling completely through bone while at the same time not striking the dura/brain is

an acquired skill and proper drill technique can only come through practice. It is possible to sense the point of breaking through by subtle differences in vibration of the skull-fixing forceps and timbre changes of the drill bit during insertion.

Insertion of screws can be completed individually (immediately after each hole is drilled) which has the benefit of ensuring proper drill depth is achieved prior to adjusting the stereotaxic arm or collectively (after all holes are drilled) which has the benefit of shortening total drill time. The method of screw insertion is left to the surgeon, but all screws should insert to a depth no less than half the total thread length and be relatively tight once fully in place. To insert, a screw is held with forceps at the base of the threads near the screw head and adequate pressure is applied through a screwdriver while driving the screw into the pilot hole all the while maintaining the previously drilled ~90° surface angle.

A sixth hole should be made for the AgCl electrode ground pellet. However due to the pellet's size, it is recommended to drill a somewhat larger hole. This can be accomplished by (after drilling the pilot hole) changing the bit in the stereotaxic arm drill or by re-drilling the pilot hole by hand with a round bit. A tight fit is not as vital for the ground pellet as for the screws so quickly drilling into the pilot hole with a steady hand is quicker and therefore recommended.

After drilling the 6 holes and inserting screws the craniotomy can be performed. Typically, a craniotomy window of 2x2 mm is used but can vary with dimensions of the probe which will be inserted. With a window of 2x2 mm the skull is opened approximately 1-3 mm from the midline and 0.5 mm anterior and 1.5 mm posterior to the bregma. Placement of the window should be marked with a Sharpie prior to any drilling to ensure proper fit and placement. Drilling of the window is done with the hand drill and an accompanying round drill bit while viewing through the surgical stereo microscope. As with drilling for screw holes, hand drilling a craniotomy window is an acquired skill and comes only through practice. However, mistakes can be minimized by shortening the lever arm of the drill (holding as close to the bit as possible), steadying wrists/arms on the stereotaxic apparatus, and drilling many shallow passes

along the perimeter of the window. Drill speed is to be decided by the surgeon. Fast drill speeds produce cleaner, more predictable cuts but can suddenly puncture thicker sections of bone which can be troublesome when nearing the surface of the brain. On the other hand, slower speeds produce rough lines (resulting in more damage to surrounding tissue) but take material away from the surface at a slower, more forgiving rate.

Once the full perimeter of the craniotomy window has been drilled through exposing the dura mater, the remaining bone fragment can be removed with forceps. If a relatively large amount of force is required to lift the bone, doing so may lead to a ruptured blood vessel or a large, unwanted tear in the dura. Application of saline solution to the window and allowing to sit (1-2 minutes) encourages the separation of the skull fragment from the underlying tissue. Finally, the bone fragment can be lifted by applying back-and-forth and side-to-side movements while simultaneously applying a gentle upward force with forceps.

With the window open and the dura mater fully exposed it is vital to the health of the tissue that the window remain fully saturated with saline until the final steps of closing with Kwik Sil (World Precision Instruments, KWIK-SIL). Therefore, if bleeding does occur from now until closing, saline saturated gel foam (as opposed to previously utilized cotton swabs) should be gently massaged into the point of bleeding until a sufficient clot is formed.

If the dura is still fully intact a tear should be made using the blunted tip of a very high (23+) gauge needle. Using the tip of the needle as a hook, the dura can be pierced, raised, and torn multiple times (parallel to the midline) producing a tear sufficiently wide enough to accommodate the MEA probe tip (~1.5 mm). Special care should be taken when tearing the dura as a punctured of blood vessels can jeopardize the health of the tissue near the implant.

The MEA probe (with headstage and anchor attached) can now be inserted into the MEA holding mechanism in the adjustable arm of the stereotaxic table. With the probe positioned close to the skull, the tips of the shanks can now be aligned with the slit in the dura and the anchor should be positioned toward the midline of the animal. Electrode orientation

(perpendicular to dorsal surface, parallel to midline) and position (0.5 mm caudal from bregma, 2 mm lateral from midline, spanning 1.4 mm in the rostrocaudal direction (figure 4)) were deliberately chosen based on previous intracortical microstimulation studies within primary motor cortex (Kolb 1990). This area is responsible for a large number of body movements including hip flexion, trunk movements, pronation, wrist extension, elbow flexion, neck movement, and vibrissa movement. The probe can then be lowered into place through the tear in the dura such that the tips of the shanks rest on the surface of the brain. After noting the reading of the depth adjustment knob on the stereotaxic arm, the probe should be lowered to a depth of 1400μm from the initial reading. During the lowering process dimpling of the brain surface, or a slight bending of the electrode shanks, will more than likely occur. If the MEA is lowered too quickly, this dimpling can cause the shanks to fold or break within the tissue leading to a damaged and unusable MEA. To remedy the effect of dimpling, the stereotaxic arm can be gently tapped with a hard object (i.e. the back end of a pair of forceps). The vibrations transferred through the stereotaxic arm encourage the relaxing of the compression stored in the shanks. With the electrode fully in place, the ground pellet can be inserted into the pre-drilled hole taking care not to bump the stereotaxic arm or strike the electrode tips.

Once proper electrode depth has been achieved, the ground pellet inserted, and all bleeding has ceased, the final steps of sealing the wound can be started. First, the wires for the probe and the ground pellet should be collected and fixed close to the MEA and anchor using a small amount of super glue if necessary. Next, a small amount (enough to fill the craniotomy window) of Kwik Sil should be applied and allowed to cure for 1-2 minutes. While waiting for the Kwik Sil to cure a small amount of dental cement can be made by mixing equal parts dry to wet material inside a small disposable cup (syringe container end caps work well for this). Once the Kwik Sil is sufficiently tacky, dental cement can be applied using a small metal spatula to the wound area starting from the center and moving outward toward the skin. Because the dental cement interacts with ambient air and hardens in roughly 1 minute, the application should be

made with relative haste while simultaneously taking caution to only apply cement to the wound/implant area.

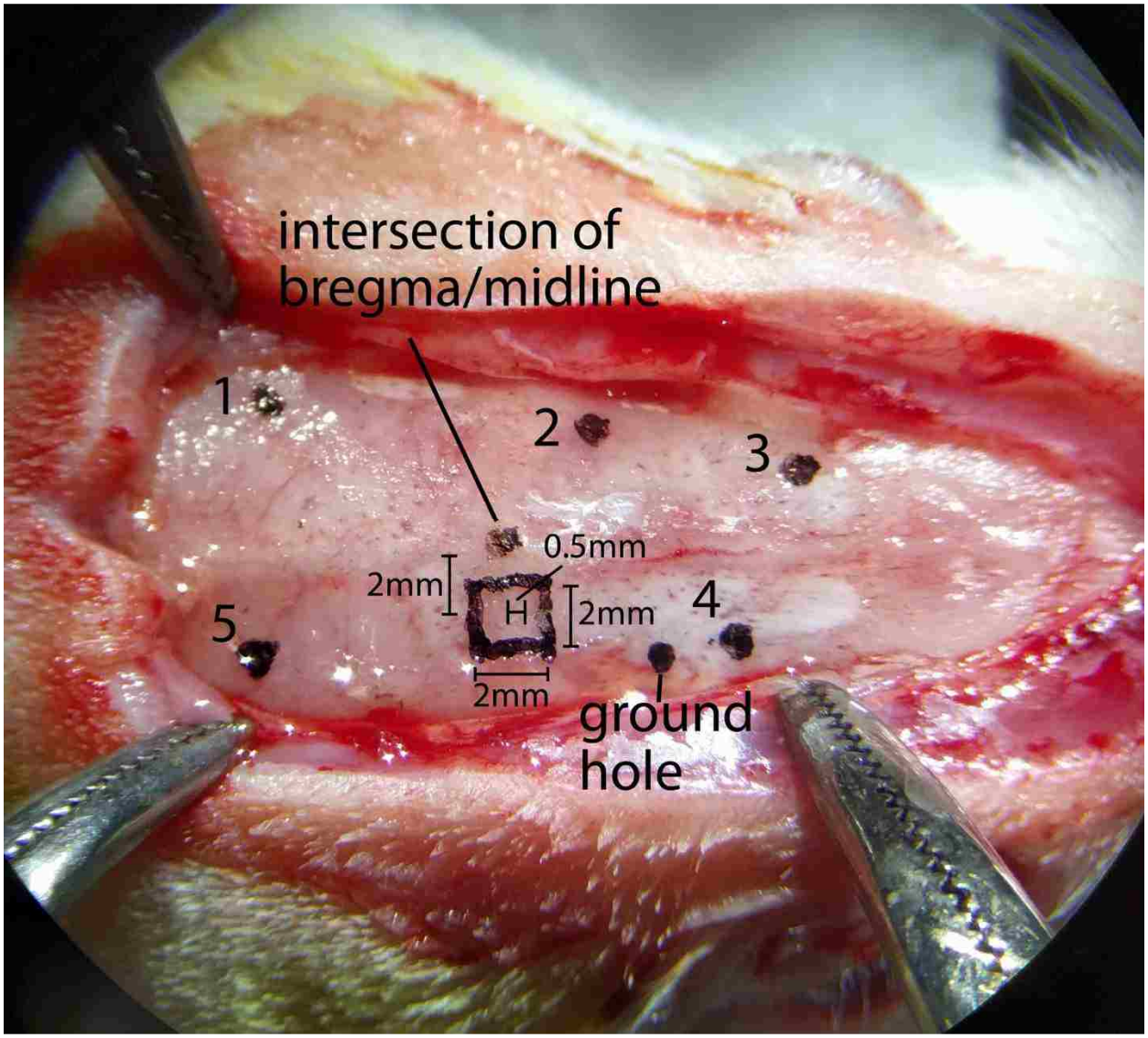

Figure 4 - Craniotomy window, screw, and ground pellet placement. For proper anchoring of the MEA implant 5 screws should be inserted to the skull around the perimeter of the opened area. A sixth hole for the ground pellet should be made near the craniotomy window. All points which will be drill should be mapped and recorded with sharpie before drilling begins to ensure proper placement and maximum coverage. Photo by Jingwen Li.

Due to the time-varying viscosity of dental cement, application to specific areas should be planned out to utilize the different stages of viscosity. Large, concave areas can be filled easily near the beginning stages after mixing whereas cementing the vertical surfaces of the

anchor requires a more stable, honey-like viscosity for sufficient coverage. Multiple batches of dental cement will need to be mixed to ensure full coverage of the implant and 4-5 small (~5 mL) batches are not uncommon. A thorough application of dental cement should extend from the perimeter of the skin up toward the midline of the anchor bottom while covering all wires and any edges of the MEA (figure 5). Because the animals will repetitively groom the area once revived, a smooth dome shaped surface is preferred which should minimize any injury caused by grooming.

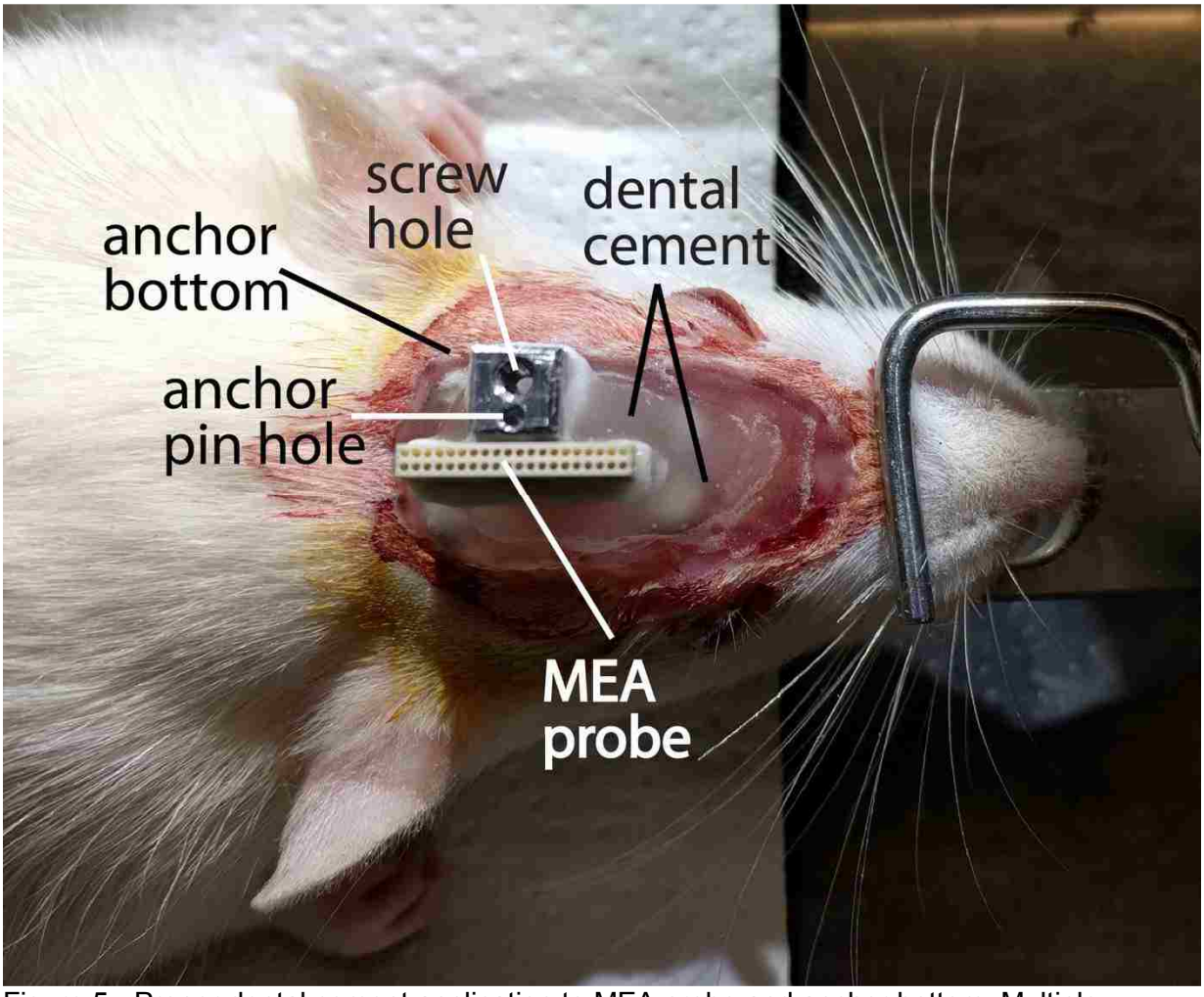

Figure 5 - Proper dental cement application to MEA probe and anchor bottom. Multiple applications of dental cement are required. Initial layers should begin at the base of the MEA and work out toward the skin surrounding the wound. Later applications should carefully be built up toward the top of the anchor and implant. Photo by Jingwen Li.

Once a thorough application of dental cement is applied and allowed to dry the animal can be placed into a high-ceiling cage for recovery. Prior to removing the animal from the stereotaxis, the isoflurane system should be turned off (along with the accompanying oxygen supply) and the thermometer probe should be removed from the animal's anus. Once placed into the recovery cage the animal should be closely monitored for the next 24 hours. Warning signs of a less than ideal surgery include, but are not limited to, very low food/water consumption, excessive external bleeding, strange motor behaviors, and excessive/abnormal sleep cycles. Two bacon-flavored antibiotic/pain relieving tablets (one dry, one moistened) along with a full bottle of water should be placed within the cage and checked the following day as a test of the rat's appetite. These two tablets (purchased from Bioserv) should be replaced (discarding any uneaten portions) every 24-48 hours or as needed and consumption should be monitored closely for the following two weeks. Depending on the health of the animal experiments can be conducted from 10 days to 2 weeks post-op.

Experimental Setup

The experiment is composed of three distinct parts: an infra-red (IR) behavior tracking setup, a neural recording system, and modulation of inhibitory signaling via pharmacological manipulation.

IR tracking

Because we are attempting to study the natural, unconstrained behavior of animals, a space for the animals to freely explore is necessary. Since the method with which we will be collecting behavior data is through the use of IR motion capture via beads attached to the body, we needed an area in which the beads will not be obscured from the view of our cameras (i.e. walls, cage bars, etc.). Therefore, a 30x30cm pedestal was constructed out of aluminum and

fixed to four posts (2 feet long) covering a 15x15cm area situated under the center of the pedestal. This smaller post area supplies enough support to the metal surface while still being narrow enough to keep animals from escaping the platform (climbing down the posts). The metal is fixed to the post via four screws and covered with black felt material which reduces reflections and acts as a buffer between the animals and the hard aluminum surface. We found that grounding the aluminum pedestal plate to the enclosure via a braided wire helped to decrease some electrical noise during recordings of neural signals.

As stated before, due to the rat's nocturnal nature experiments must be performed in low-light conditions for sufficient behavior activity to be recorded. Therefore, the pedestal is surrounded by a light-proof enclosure. This enclosure (55x47x54 in.) is made up of a metal frame (80/20 aluminum) with large slabs of thick black poster board which are cut and permanently fixed to three sides as well as the top of the frame. Any areas which cannot be covered via poster board are thoroughly patched with black felt. The fourth front-facing side of the enclosure should be covered with one large removable piece of poster board. The front side must be accessible to allow for adjustment/calibration of the cameras as well as insertion of animals for experiments.

The motion capture system is composed to 9 IR emitting cameras (Flex 3 model via OptiTrack), Motive tracking software (OptiTrack), and 3mm reflective markers (OptiTrack, part number: MCP1125). Prior to experiments cameras must be fixed along the perimeter of the aluminum frame and calibrated for recording (figure 6). One camera is sufficient for capturing the bird's eye view of the pedestal leaving 8 to be spaced relatively equidistant along the sides of the frame. The cameras should be elevated with respect to the pedestal by an amount which gives them a viewing angle of roughly 20 degrees below the horizontal when focused on the center of the pedestal. Because the markers will be placed along the back and sides of the animal, this downward facing angle provides exposure to a larger number of dots for each camera.

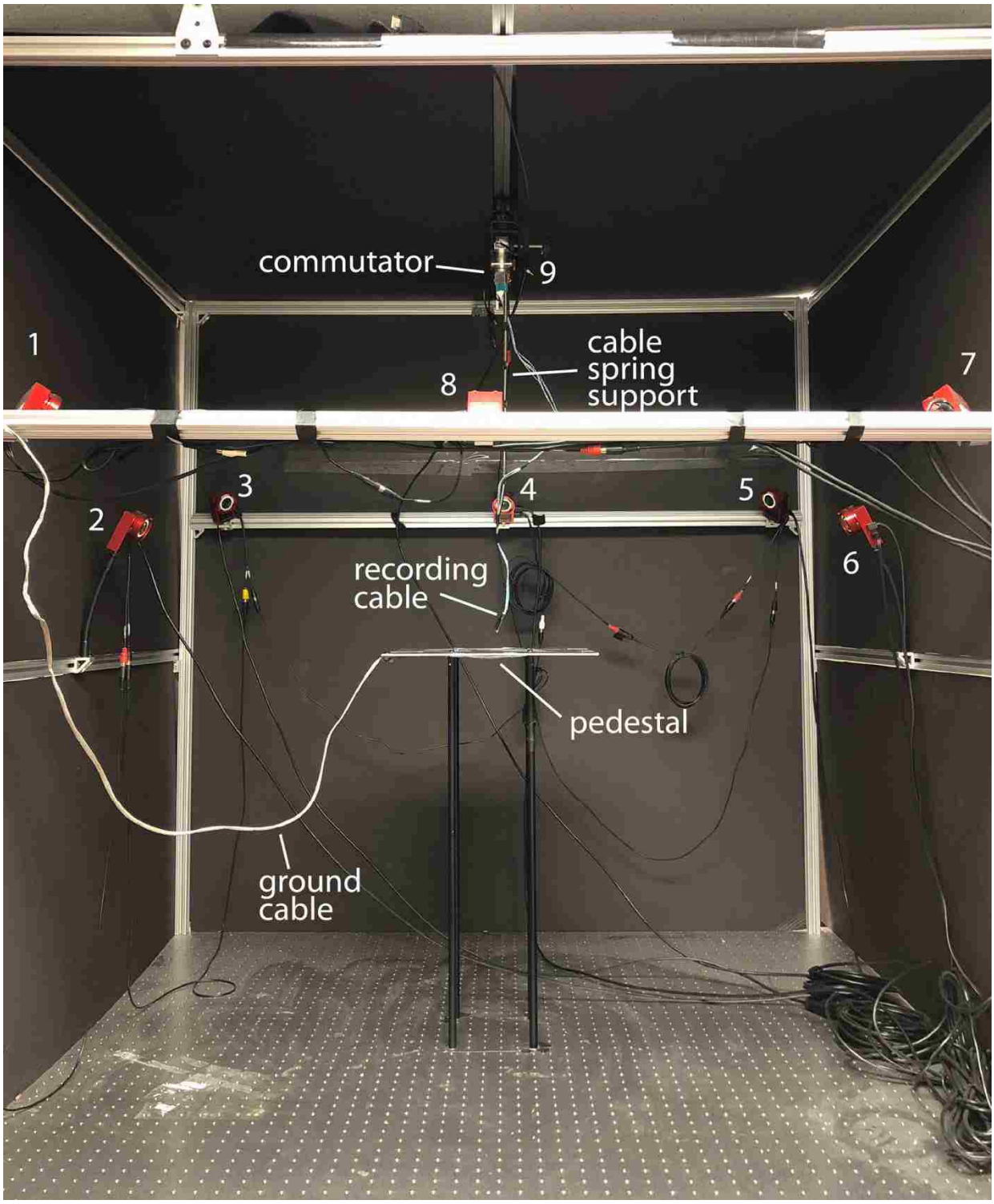

Figure 6 - Camera placement inside recording volume. Cameras are fixed equidistant along an aluminum frame. They are positioned at heights such that the angle their perpendicular makes with the pedestal is ~20 degrees for optimal recording volume coverage. The neural system recording cable extends from a free-moving commutator. The cable is suspended with a spring mechanism which supports the weight of the cable allowing free, unconstrained animal behavior.

The cameras collect 3D motion data by triangulating 2D data from multiple cameras. Because the cameras cannot sense depth but can give accurate readings of dot placement in a plane, these 2D planes can be combined and 3D coordinates of the dots can be extrapolated if the distance between cameras is known. Therefore, once all cameras are fixed into their permanent locations, the first step in recording is calibrating the camera system to accurately calculate inter-camera spacing. A calibration wand with three markers is supplied by OptiTrack and should be utilized for the calibration process. OptiTrack software does all the triangulation automatically.

Upon opening the Motive software, a selection box is prompted to the user with several options: Open existing take, Open new take, Camera calibration, etc. After selecting the 'Camera calibration' option the camera views will undoubtedly be overexposed and messy. Some adjustments can be made to reduce noise and give a clearer picture of the recording volume. First, IR mode should be set to strobed for the system. Next, threshold, exposure, and LED should be adjusted for each camera independently until several dots placed on the pedestal appear as small, discrete objects. The values of the aforementioned variables should be recorded for ease of calibration in the future.

Table 1: Camera exposure, threshold, and LED setting for motion capture system.

Camera number	Exposure	Threshold	LED intensity
1	98	200	4
2	98	200	5
3	98	200	3
4	98	200	4
5	98	200	2
6	98	200	4
7	98	200	3
8	98	200	3
9	98	200	5

Initially, several cameras will capture one or more of the other cameras' LEDs in their field of view, causing the software to incorrectly identify some of these LEDs as markers to track. To avoid this, the 'block current markers' button should be clicked which permanently

blocks these areas and reduces false markers produced by the IR emitted by other cameras. The system is now ready to be calibrated.

After the correct wand size is selected (250mm in these experiments, OptiTrack, part number: CWM-250) the ‘Start wanding’ button can be clicked and the wand can be simultaneously waved and rotated throughout the recording volume until sufficient coverage (denoted by ‘excellent’) is attained on most, if not all, camera calibration boxes. This step should be completed with the pedestal removed as it would obstruct the motion of the wand throughout the volume. Next, the ‘calculate’ button should be pressed and a ‘very good’ or better valuation of calibration should be achieved before continuing. Once wanding and calibration are complete, Motive will then prompt the user to set the ground plane for recording (this designates where ‘0’ is on the vertical axis) at which point the pedestal should be put into place and the ground plane tool (small pronged object with 3 markers forming a right angle, OptiTrack, part number: CS-100) should be placed on the pedestal and the ‘set ground plane’ button can be clicked. If successful, the calibration can be saved in the ‘Motive calibrations’ folder. If the cameras are not moved or adjusted from this point on, the same calibration file can be used for multiple recordings. However, calibrating cameras every few recordings will reduce errors caused by slight movements to cameras due to vibrations and/or accidental movements during removing and replacing the front poster board panel of the enclosure.

The calibration file can now be used as an ‘existing take’ when opening Motive. The calibration file should open with all camera presets saved and any exposed cameras ‘blocked’ and therefore ready to record data. The process of recording during an experiment is simple, when the large red ‘record’ button is pressed a new take with its corresponding date and time is created. When the large ‘stop recording’ button is pressed (the record button is replaced with this during active recording) the take ends and no further data can be added to the take. Instead, any subsequent ‘record’ and ‘stop recording’ clicks create and end new takes. Once a recording is complete, it should be saved as Motive (and most CPU intensive software) can

sometimes crash resulting in total loss of any cached data. Once saved, Motive can be shut down and the fresh calibration file can be used or multiple takes can be taken and ultimately saved as a 'project'. Project files contain all tracking files that were taken during an extended recording session (e.g. all files for a single experiment day).

Neural recording system

Extracellular voltages are recorded from the MEA via a Blackrock Microsystems recording setup that consists of a main computer (running Windows) and a Cerebus Neural Signal Processor (NSP) which collects neural signals from the analog-to-digital headstage/amplifier which is connected to the MEA probe. The signals from the headstage are fed through a freely-rotating commutator mechanism positioned above the pedestal and the connected wire is supported via a spring mechanism (figure 6) which decreases the weight of the wire on the animal's head implant allowing for more unconstrained movement.

While the Blackrock system is able to simultaneously process 96 channels and isolate spike waveform data in real time, this particular experiment requires only the raw signal from 32 channels. Therefore, the first and possibly most important step in setting up the system for recording is to set the data filtering option to 'none'. The file path should be set prior to recording and a consistent and clear naming scheme or nested folder path should be used for labeling (e.g. Rat2_041617_muscimol). Once any filters are removed and the animal is connected via the headstage data can be collected via the large red 'Record' button.

Results of this experiment depend heavily on time-locked, simultaneous data series from the body and cortex of animals. However, the recording setup consists of two separate computers and therefore two distinct recording softwares with their respective 'Record' buttons. The simplest approach to syncing the systems was used, that is, the recorder would click 'Record' on both systems simultaneously. Although this method will never ensure perfect

simultaneity, differences in start and stop times of less than 0.25s are easily achievable (determined from recording clocks).

Inhibitory modulation

In order to test what role inhibitory signaling plays in motor function and control, it is necessary to pharmacologically modulate the strength of these inhibitory pathways and in turn capture a broad set of neural and corresponding behavior data sets for analysis. The initial experimental design accomplished this by globally affecting inhibitory signals by way of intraperitoneal (IP) injections which not only affects neurons in the central nervous system (CNS) but also the peripheral nervous system (PNS). Global inhibitory modulation, while technically simple, left many fundamental questions unanswered and was therefore replaced by a technique which allowed for local inhibitory modulation in cortex alone.

Global modulation

As stated previously, global inhibitory modulation is achieved via IP injection which is the process of injecting fluid into the peritoneum, or body cavity, of the animal. The injected fluid eventually diffuses throughout the organism to affect target cells which are specific to the injected chemical.

All pharmacological manipulations in our work targeted $GABA_A$ receptor sites. Both excitatory and inhibitory neurons have such $GABA_A$ receptors. Muscimol, which is a $GABA_A$ agonist, increases the strength of inhibitory signaling and was used at a strength of 2mg/kg bodyweight during IP injections. On the other hand, inhibition was decreased by way of pentylenetetrazol (PTZ), a $GABA_A$ antagonist at a similar concentration of 2mg/kg bodyweight. Drug concentrations were tested independently and found to induce sufficient behavior changes at these concentrations. Large batches of drug solutions can be prepared in advance and stored

in a refrigerated environment for weeks at a time. Drugs should be checked for contaminates prior to use. If any particulates are suspended within the solution, the drug should be replaced as any macro sized objects indicate the presence of contamination. The drugs are mixed with saline to form a solution with a known chemical concentration, typically 1-2mg of drug to 1mL of solution. This concentration translates to 0.3-0.6mL of injectable volume for a typical 300g rat. Along with drug injections saline sham injections (no drug) were administered each experiment day. These sham injection recordings served two purposes: a baseline for the animal's current state on a particular day, and they also accounted for pain or discomfort caused by an IP injection.

In order to administer an IP injection, the animal should be thoroughly anesthetized via the isoflurane system (as outlined in the surgery section). Prior to anesthesia, the injectable volume should be drawn into a syringe with a 25 (or higher) gauge needle and placed nearby with the needle covered with the syringe cap. Once properly anesthetized, the animal can either be turned upside down on a tabletop, or preferably held upside down in the experimenter's non-dominant hand with the head directed away from him/her. The syringe should then be gripped with the dominant hand and cap removed. The needle should be carefully slid under the animal's skin near the stomach region. Needle insertion should be made somewhat parallel to the skin of the animal, to ensure the drug is administered into the body cavity and not a vital organ. Injecting either drug into an organ could result in a fatality and therefore it is important to take caution when injecting. Once the needle is inserted and one is sure the drug will be injected into the peritoneum, the syringe should then be aspirated. Aspiration is the act of pulling back on the plunger of the syringe and ensures the tip of the needle is not inserted into a vein or artery. If aspiration results in blood filling the tip of the syringe, a vein or artery was punctured and the syringe should be discarded, a fresh syringe prepared, and a second attempt can be made. If instead a small air pocket fills the tip of the syringe, the solution can safely be injected into the peritoneum slowly over a 2-3 second period.

Once injected, sufficient time should be given for the drug to diffuse throughout the body and fully effect the animal's nervous system. Rats should be placed in their cage after injections and allowed to rest for a minimum of 30-minutes prior to recording. This waiting period, though pharmacologically unnecessary, is carried over into the control group (saline sham injections) for consistency of methods.

Local modulation

Local inhibitory modulation is achieved by way of micro-fluid injections via cannula (33GA internal cannula inserted into a 26GA guide cannula, Plastics One, Roanoke, VA) which is implanted near the MEA electrode probe during surgery. Drugs are diffused directly onto the surface of the cortex via a microfluidic syringe pump (Bioanalytical Systems, Inc., IN) which delivers small volumes (1-2 µL) of solution at a rate of 0.2 µL/minute over 5-10 minutes.

As with global inhibitory modulation, local injections target inhibitory cells with $GABA_A$ receptors and thereby modulate inhibitory signaling in cortex. Muscimol was used again to increase inhibitory connection strengths. However, because there is not sufficient literature on direct injection of PTZ in cortex, bicuculline, a more thoroughly vetted (Matsumura et al. 1991) [Matsumura] antagonist with similar $GABA_A$ receptor action was substituted to modulate inhibition locally. Both drug concentrations were increased on a weekly basis from 20-1280 µMolar by doubling the previous week's concentration (20 µM, 40 µM, 80 µM, etc.). At the beginning of each experiment week specific drug concentrations (as we all saline for sham injections) can be mixed and inserted into the special syringes which accompany the microfluidic pump. The drugs contained should be stored in a refrigerated environment prior to- and after completion of experiments. The 5mL capacity should be sufficient to carry out four experiment days with two rats per week after which they should be thoroughly cleaned with saline and stored in preparation for the next week.

At the beginning of the day, two syringes (one saline, one drug specific to that day's experiment) should be removed from the refrigerator, inserted into the microfluidic pump, and allowed to come to room temperature. A number of cannula tips and screws corresponding to the number of recordings that will take place that day should be removed from the bottle of alcohol, dipped in saline, and allowed to dry (reserving several extras in case of accidental contamination during handling). For drug administration, the animal is once again thoroughly anesthetized but due to the longer administration time, the animal is placed in the stereotaxis and isoflurane is continually administered. With the animal safely inside the stereotaxis, the cannula screw can be removed and replaced into the bottle of alcohol and a cannula tip should be inserted onto the end of the syringe hose for the corresponding drug condition and flushed for a short time (3-5 seconds) with the pump set to a very high flow rate (~20 µL/min). With the flow turned off and the flow rate set to 0.2 µL/min, the cannula tip can then be inserted into the cannula until a proper seal is formed (designated by a clicking or snapping sensation). After starting a timer which will account for the total volume to be injected, the pump can be turned on and allowed to infuse the desired volume of solution (both 1 or 2µL in these experiments depending on drug concentration). After infusion, the cannula tip should be removed, stored in a bottle of alcohol, and the cannula should be sealed with a fresh cannula screw. Because the drugs are diffused directly into the cortex tissue, a waiting period is unnecessary and (once the animal has recovered from anesthesia) recordings can be carried out immediately.

Performing an experiment

Once rats are fully recovered from their chronic implant surgery experiments can begin. Animals are housed in the CLAF animal care facility and must be brought from- and returned to the CLAF facility before and after all recordings. Multiple animals can be recorded from in a single day by designing a block-style recording schedule as outlined below.

Table 2: Block drug administration/recording schedule for global inhibitory modulation.

	T+0:00-0:30	**T+0:30-1:00**	**T+1:00-1:30**	**T+1:30-2:00**	**T+2:00-2:30**
Rat 1	Saline injection	Record	Drug injection	Record	
Rat 2		Saline injection	Record	Drug injection	Record

Table 3: Block drug administration/recording schedule for local inhibitory modulation.

	T+0:00-0:30	**T+0:30-1:00**	**T+1:00-1:30**	**T+1:30-2:00**
Rat 1	Saline injection & record		Drug injection & record	
Rat 2		Saline injection & record		Drug injection & record

Experiments consist of two consecutive recording days, each day having two separate 30-minute recordings (one saline-sham an one drug condition). Recording days are typically two days on, one day off, two days on, two days off. This schedule offers sufficient recovery time from bouts of pharmacological manipulation as well as having the added benefit of structuring neatly into an average work-week. Regardless of the method of inhibitory modulation, inhibition was always decreased on the first day of recordings and increased on the second. Also, both drugs were never administered on a single day.

Once animals are weighed and secured safely in the surgery room, drugs for that day are taken out of refrigeration and allowed to come up to room temperature. During this time there are several small tasks that must be completed before recordings can be started. The black felt on top of the pedestal should be replaced with a fresh piece and the old discarded in the large cardboard ‘biohazards’ container. The recording softwares should be primed for recording by setting up file path locations and making any other necessary initial adjustments (camera settings, personalized screen layouts, etc.). If doing local pharmacological manipulation, clean accessories for the cannula should be prepared and set aside. If IP

injections will be administered, drugs (once completely thawed) can be portioned into syringes and set aside. The anesthesia system can be cleaned and, if necessary, isoflurane added to bring the indicator to its fill line.

With all preliminary steps taken care of either of the aforementioned recording schedules may be started. For simplicity sake, I will describe the steps carried out in a single recording. All steps remain the same for both styles of recording with the exception of when and how drugs are administered (as seen in tables 2 and 3 outlined above).

The animal is initially sedated using the isoflurane station and transferred to the stereotaxis table wherein the 8 reflective beads are placed on the animal's body (6 evenly spaced along the animal's spine from several mm ahead of the front shoulder blades to the base of the tail, and two on the rear hips, figure 7). Also, if inhibition is being modulated locally, the process should be initiated prior to the placement of the beads to minimize wasted time. Once the beads are properly positioned and firmly affixed (and any cannula work is completed), the MEA dust cap (maintains cleanliness of probe when not in use) should be removed and the headstage firmly connected to the MEA. The headstage support screw should then be screwed into the anchor bottom on the implant. After turning off the isoflurane system, the animal can be placed back into an open-top cage and transferred (in an opaque container, e.g. a cooler bag) from the surgery room to the recording room. The cage should be placed on the pedestal and the headstage securely attached to the NSP wire which runs from the commutator to the stage. Once fully recovered from anesthesia (3-5 minutes), the animal can be placed on the pedestal (by lifting at the base of the tail and sliding the cage out from underneath) and observed closely for 1-2 minutes ensuring proper wakefulness before placing the front-side wall of the enclosure on the metal frame.

With the animal in place the recording should begin as soon as possible. Because separate recordings (neural and body) are done on two independent devices, one should attempt to press both record mouse-clicks simultaneously. Because both computers internal

clocks have the same pace, a small, constant lag in one data set with respect to the other should not affect results. If there is an obvious discrepancy between the two recording times the recording can be deleted and restarted until a respectable tolerance is achieved (<~0.25s).

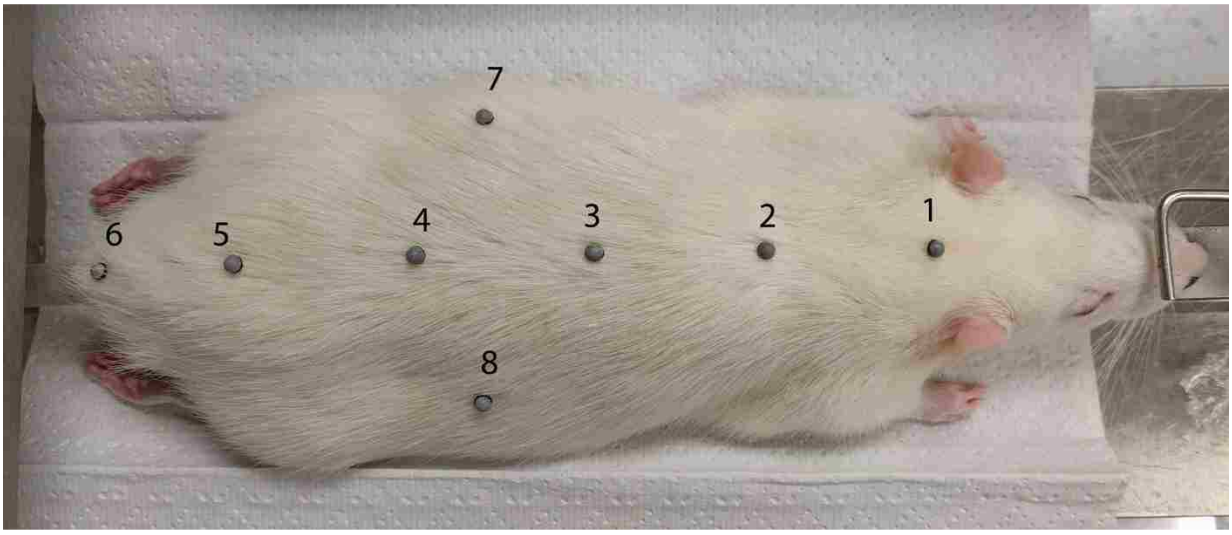

Figure 7 - Bead placement along posterior side of animal. Trial and error resulted in the above bead placement which ensures consistent tracking throughout recordings. Photo by Jingwen Li.

Data should be taken for no less than 30-minutes. During this time, the animal should be observed and notes on behavior as well as any possible spiking channels should be recorded and reflected on during data analysis. Once recording is complete, both softwares can be stopped and the file path for the following recording can be set in advance.

The enclosure can then be opened, and the connector quickly separated from the headstage. After moving the top of the cage to the side of the pedestal and tilting at a large angle, the rat can be gently coaxed into walking down the side and onto the bottom of the cage. Once placed back into the opaque transportation container (i.e. cooler bag), the rat can be transferred back to the surgery room and anesthetized. After anesthetizing, an IP injection can be applied (if modulating inhibition globally) then placed directly into the stereotaxis to remove the reflective beads and the headstage. The dust cap should be replaced over the MEA using the metal cover and securely fixed with the anchor screw. The animal can then be transferred back to a secure (closed-top) cage with sufficient chow and water.

When all recordings have been completed for the day, the isoflurane system (along with the oxygen bottle) should be double-checked to ensure everything is in the ‘off’ position. The animals should be returned and placed into separate cages in the CLAF facility before the workday is complete. Cages should be checked for proper chow and water (lightly squeezing the water bottle will ensure it is free flowing and without any obstructions) and cooler bags can be stored inside the respective animal care rooms for future use.

Data analysis methods

Bead labeling and editing

Post-processing of raw position files can be completed in Motive's 'Editor mode'. The goal of post-processing is to consistently label and track individual beads throughout entire recordings or 'takes'. In other words, individual bead data should be 'gapless' and the initially specified numbering scheme (1-6 along the spine of the rat with 1 being at the base of the neck and 6 at the base of the tail, 7 and 8 are placed on the left and right biceps femoris respectively) should remain fixed.

Once calibrated properly, the IR motion capture system uses triangulation techniques to obtain 3D data via simultaneous images provided by multiple cameras within the system. Due to obstructions during recording sessions (the rat's body, recording cable, etc.), individual beads within the recording volume are occasionally tracked by fewer than 2 cameras which is the minimum required for triangulation. When this occurs, the bead will disappear from the take and reappear once it is tracked by multiple cameras. If a number was assigned to the bead prior to its disappearance, that information must be added to the 'new' bead in a consistent manner.

Prior to labeling beads, a marker set must be added to the take and then the take can be trajectorized. Adding a marker set is done by clicking the 'add marker set' icon above the 'take' dialog box. The new, empty marker set should appear in the lower left corner. It can be populated with the values 1-8 (or any other sensible naming scheme) by right clicking inside the empty area, labeling the new marker, and pressing enter. Once all markers are added the marker set should be clicked and dragged to the take. After adding the marker set to the take, 3D data can be calculated from the raw recording data by right clicking the take name and selecting 'Trajectorize take'. Once trajectorized, a large number of markers sets should appear in the editor window.

The simplest method for labeling beads through an entire take is to simply scrub through the recording while simultaneously viewing the editor window. After labeling all 8 beads at the beginning of the recording (by simply right-clicking a bead, selecting ‘label marker’, and selecting the appropriate number), 8 green rows should appear in the editor window. These provide a visual representation of bead tracking throughout the recording. with shorter rows representing those beads which were not tracked as long as others. Therefore, by scrubbing to the end of the shortest row, that bead can be re-labeled once it returns to the recording, adding to its length. This process should be continued until the end of the recording is reached and all 8 beads are consistently labeled throughout the recording.

Due to the beads’ disappearance throughout the recording there will inevitably be small gaps in the tracking data. Typical gap length is on the order of 10s of milliseconds. These gaps correspond to ‘flickering’, or quickly disappearing and reappearing within the field of view of a single camera (obstructed due to recording cable or animal hair, limbs, etc.). These gaps can be filled by using the ‘Gap fill’ panel in the editor. ‘Linear’ fill should be selected and a large, default gap size can be input (e.g. 10000 frames) by the user. After selecting a bead which contains gaps (designated with a ‘G’ in the marker set panel), next or previous gaps can be jumped to by pressing ‘find next’ or ‘find previous’. Gaps which are larger than the range set by the user will not be found, therefore the large default size is required to visualize all gaps in the recording. With a gap highlighted, the ‘fill gap’ button can be clicked and the gap should automatically be filled. The software is able to accurately fill smaller gaps (~10-20 frames) to a very high degree of accuracy. However, if the gap is too large the filled data may be very inaccurate. If this is the case, the bead should be removed from the entire recording. This deletion does reduce the dimensionality of the collected data but this reduction in dimensionality is preferred to what would be a large amount of falsified data. On average, 1 out of roughly 20 recordings required the deletion of a single dot.

After filling all gaps throughout the take the extraneous marker sets can be deleted leaving only those markers along the backside of the animal throughout the entirety of the recording. The tracking data can be output (File>Export tracking data…) using a consistent and clear naming scheme or nested folder path for labeling (e.g. Rat2_041617_musc). Files should be saved to a comma-separated values (.CSV) format at a 'Recording rate' of 100Hz. Along with 3D coordinates for all beads, .CSV files contain header information which explains in detail the contents of the files.

Spike sorting

The neural recording system acquires raw extracellular voltage signals from the 32-channel probes at 30k samples/second. These raw voltage signals contain a wealth of information that can be interpreted in a number of ways. This work uses extracted single unit spiking activity, that is, times of action potential events for detected neurons throughout recordings. Therefore, prior to analysis, single unit spiking activity must be extracted from these extracellular voltage signals.

There are a number of spike sorting software suites on the market but they all process the raw data in a similar fashion. First, raw voltage signals are band pass filtered to cut out frequencies which are either lower (<250 Hz) or higher (>5000Hz) than the typical frequencies associated with action potentials. Then, voltage threshold values are set. When the voltage falls below or rises above (or a combination of the two) the threshold value (called a 'threshold crossing'), the software will extract a short voltage time series (predetermined number of samples) centered about the threshold crossing. This set of voltage samples is called a 'spike waveform' due to its classic spike-like appearance. These spike waveforms are collected, or 'cut', for all threshold crossings across all channels for the duration of the recording. Finally, principle component analysis (PCA) is used to isolate the spiking activity of individual units from

noise artifacts, and in some cases, the activity of other neurons recorded on the same channel. The end result of the spike sorting process is an array of unique unit IDs with corresponding spike event times.

Offline Sorter

Offline sorter is a proprietary spike sorting software (Plexon) which requires a USB hardware key. Prior to sorting spikes in Offline Sorter spike waveforms must be cut from the recordings using the Blackrock Cerebus system used to acquire the raw voltage signals during experiments.

After loading the appropriate recording file into the NSP software and clicking the 'Play' button, spikes can be visualized in the 'Spike Panel'. Double-clicking a channel window opens a new window which displays spiking activity for that single channel. The voltage threshold slider can then be adjusted to maximize the collection of spikes while minimizing extraneous noise. Since the shape (duration, peak values, etc.) of any two neurons is dependent on the neuron as well as the distance from the electrode, threshold crossing values should be set for each channel independently.

After setting the thresholds for all channels, spike waveforms can be cut from the recording. First, the timeline scrubber should be returned to the beginning of the recording and the play speed can be adjusted to its highest setting. A file path and name should be set and the 'extract spikes' checkbox enabled. After initiating the recording then pressing play, the recording should be allowed to play out in its entirety after which point the recording can be stopped.

The spike waveform file can be loaded into Offline Sorter where spiking activity on each channel can be viewed in PCA space. Principle component analysis is the process by which a collection of waveforms are broken down into similar fundamental waveforms, or principle components. Therefore, any waveform in the original set can be reconstructed as a linear

superposition of these principle components. The superposition of an individual waveform can be visualized as a point in principle component space.

After selecting a channel from the drop-down menu, the spike waveforms collected from the channel will appear as points in the user selected PCA space. Offline Sorter allows the user to use the three dominant principal components as well as other features of the spike waveforms (e.g. peak-to-peak amplitude, peak-to-trough duration, etc.) which best separates, or 'clusters', neuron spiking information from noise information. Spikes can be selected (and subsequently removed) by clicking the 'Add WFs' and 'Remove WFs' buttons and drawing around clusters which correspond to spike data. If multiple units were recorded from a single channel, clicking the 'Add unit' button creates a second unit to which waveforms can again be added.

Once all spiking units across all channels have been labeled, the spike times array can be output to a .csv file by File>Export… and selecting the desired options in the dialogue box. Typically, Unit ID and Spike times is all that is required for analysis with spiking units however there are some options that may be useful for future analysis techniques (channel number, various principle components, etc.).

Klusta

Klusta is an open-source suite of tools developed by the University College London group headed by Matteo Caradini and Kenneth D Harris. The suite, which is written in python, is designed to make the spike sorting process as automated as possible. This automation has been shown[1] to improve results when compared to more involved, 'hands-on' approaches (such as the Offline Sorter method outlined above).

The software is designed to handle recordings with a few dozen probes and works best when spacing between recording sites is very small (less than about 100 microns). This small

inter-electrode spacing allows for more accurate results during the automatic clustering process (PCA analysis) due to simultaneous single spike detection across neighboring recording sites.

Once properly installed, Klusta automatically detects and sorts spikes into individual clusters via data contained in the raw voltage recording by way of user defined probe and parameter files. The probe file contains physical dimensions and geometry of the probe used during extracellular voltage recordings. The parameters file sets specifications for dozens of adjustable parameters for detection and clustering including basic recording parameters, filtering frequencies, voltage thresholding values, etc. The three files used with Klusta should be contained within their own directory since the sorting software will create a batch of files which are named using a consistent scheme, therefore overwriting and other errors can be encountered if multiple instances of the software are run in the same directory. The construction of these files is outlined below.

During recordings, the Blackrock Cerebus system saves raw voltage signals using the .NS5 file format. However, Klusta accepts flat binary files with extension .dat. Blackrock provides a package of Matlab post-processing tools which can be requested from their support staff. One useful tool within the package is the openNSxHL function which takes as input a .NS5 file which the can then be written to a new, user-defined .dat file.

The probe file contains the list of channels, an adjacency graph between the channels and the 2D coordinates of the channels. The list of channels is simply a numbering of the probe sites (0-31 for a 32-channel probe) which will be referenced in the adjacency graph and 2D geometry coordinates. The adjacency graph outlines the nearest neighbors for each recording site. The adjacency graph is used by the algorithm for triangulating simultaneous spikes recorded from multiple channels. Finally, the 2D coordinates of the channels is used for visualizing and confirming clusters of spikes in the final ‘manual curation’ step using the GUI ‘KlustaViewa’. Once constructed in a text editor, the file should be saved with the .prb extension.

The parameters file contains a number of parameters which are fully adjustable. An explanation of some of these parameters, along with a sample parameters file can be found in the Klusta documentation (www.klusta.readthedocs.io). A large portion of these parameters should remain constant from one recording to the next (Filtering, Chunks, Connected component, etc.). At the top, the parameters file contains the specific experiment to call for analysis. This must be changed for every parameters file used as each experiment should have a different filename (unless renamed after recording). The strong and weak thresholds ('threshold_strong_std_factor' and 'threshold_weak_std_factor') may need to be adjusted based off the final quality and number of clusters. These strong (and weak) thresholds determine how many standard deviations above (or below) the mean the voltage must reach before a spike is detected. For more details on how the software uses the two thresholds, see reference (Rossant et al. 2016). The more extreme (higher) these thresholds are set, the less spikes will be detected and therefore a lower number of clusters will be detected and saved in the final output. Each of these clusters corresponds to a single spiking neuron, therefore a cluster count of <100 is acceptable for data recorded from a 32-channel probe. Once constructed in a text editor the parameters file should be saved with the .prm file extension.

Once the .dat, .prb, and .prm files are constructed (see appendix for example code) and placed into a unique directory, the automatic detection and clustering can be initiated through a command prompt. After navigating to the proper directory, running the command 'klusta yourparametersfile.prm' with 'yourparametersfile' replaced with the appropriate filename should start the spike detection process. The command prompt updates with percentage completed as well as the time remaining to complete detection. Also, a number of files and folders should have been created in the directory. Once all spikes have been detected for the recording, Klusta will automatically begin the clustering process. The command prompt will frequently update with cluster scores as well as any clusters that were ultimately grouped together. Again, the directory

will contain several more files indicating the program has entered clustering mode. Once finished, the command prompt will display ‘Clustering finished!’ along with the elapsed time.

The final step of manual curation can be initiated by entering ‘klustaviewa yourkwikfilename.kwik’ with ‘yourkwikfilename’ replaced with the appropriate filename. The GUI should automatically be populated with the full set of clusters contained in the ‘unsorted’ category. If the GUI displays an error upon opening (‘No clusters’) or the set of unsorted clusters is very large >100 or very small <5, the thresholds within the .prm file should be adjusted (either up or down) such that a usable number of clusters (~5-100) are detected during the clustering process. The choice of min and max cluster numbers is dictated by the size of the probes used; through typical spike sorting methods it is not common (though still possible) to see >1 spiking unit per channel. Because we are using 32 channel probes, a soft cap of 32 clusters is expected. The reason ~75 clusters is allowed during the clustering phase is for the passage of more actual spiking cluster to pass the clustering test (and inevitably more noise clusters). However, any extra noise clusters are easily removed during the manual curation phase (outlined below).

Manual curation is the process of manually distinguishing those clusters which represent actual firing neurons from clusters which are actually noise. There are several tools available to help distinguish spiking neurons from noise.

The first, and most noticeable tool, is the ‘WaveformView’. This pane shows a 2D physical representation of the probe along with spike waveforms across all channels. The colored waveforms are spikes within the cluster in question and any gray waveforms designate activity across the channels which occur simultaneously with the detected spikes for that cluster. An actual spiking neuron should be localized in space and have a somewhat typical spike waveform shape. Noise, while possibly having the shape of a spike due to proper threshold crossings, is typically evenly distributed across a shank (or entire probe). Because voltage

fluctuations due to a firing neuron are localized in space and should decrease with distance, any constant voltage fluctuations through space cannot be representative of firing neurons.

Klusta also displays PCA space in the ‘FeatureView’ window. This is analogous to the PCA space seen in Offline Sorter, however the dimensionality is much less. The user is able to view spaces based on only the first three principle components of spike wavforms. As with Offline Sorter, spiking neurons should form clusters within these PC spaces. If the cluster passes the requirements in the WaveformView pane but spikes are not concentrated in any spaces in the FeatureView pane, the cluster should be analyzed in the ‘CorrelogramsView’ before making a final decision.

The CorrelogramsView looks at spiking activity with a 200ms window centered on each spike in the cluster. These 200ms are separated into 100 2ms time bins and spikes on either side of the triggering spike are collected within these bins. Due to the refractory nature of neurons, it is uncommon for a neuron to spike twice within a 2ms period. Therefore, if there are any spikes counted in the center timebins, the cluster has a very high chance of being constructed from noise waveforms.

If a cluster is thought to be noise it can be sent to the multi-unit activity (MUA) category by pressing ‘Delete’ when highlighted, or by right-clicking the cluster and selecting ‘move to MUA’ or ‘move to Noise’. Both the MUA and Noise categories are not extracted during analysis so either will suffice for noise clusters. Once all noise clusters are filtered removed from the Unsorted category any similar clusters that represent the same neuron can be grouped together.

The ‘SimilarityMatrixView’ pane makes visualizing similar clusters very easy by allocating all clusters and their possible matches into a square matrix with entries colored by a heatmap. Cluster combinations which are very similar are colored in warmer colors whereas those clusters which are not similar are colored with cooler colors. Right-clicking on an entry within the matrix opens the combination of both clusters in the previously mentioned views and

can be compared. If the waveforms and clusters look similar in the WaveformsView and FeatureView panes and there are no spikes in the middle bins of the CorrelogramsView, the clusters can be safely grouped by pressing ‘G’ or selecting Actions>Group Clusters. Once all noise clusters are removed and similar clusters are grouped together, all clusters in the ‘Unsorted’ category can be moved to the ‘Good’ category and the file can be saved. Neuron IDs and corresponding spike times can now be extracted from the .kwik file.

Dimensionality reduction of raw data

After spike sorting and correcting gaps in the body motion tracking data, we next sought to reduce the dimensionality of these datasets to make our data analysis simpler. For the body motion data, we began with three-dimensional coordinates of 8 marker beads (i.e. 24-dimensional data). Prior to reduction in dimensionality, bead positions were low-pass filtered with a cutoff frequency of 5 Hz. This filtering smooths any discontinuities in the position data which might result in extremely high, and nonsensical bead speeds (see below). To reduce the dimensionality, this position data was transformed into a one-dimensional timeseries of body speed averaged over the 8 marker beads. The first step in this analysis is to transform the collected position measurements into velocity, or speed (since we are uninterested in specific directional movements) data. This is computed by taking the derivative of the position data with respect to time.

$$S = \frac{|\overrightarrow{\Delta x}|}{\Delta t}$$

Computing the change in position of a single bead is given by the Pythagorean theorem in 3-dimensions:

$$|\overrightarrow{\Delta x}| = \sqrt{\Delta x^2 + \Delta y^2 + \Delta z^2}$$

where Δx, Δy, and Δz are, respectively, the change in x, y, and z coordinates of a bead.

The camera system records at 100Hz (giving a time resolution of 0.01s) with sub-millimeter spatial resolution. However, our analysis does not require data with such high precision. Therefore, both time and space are coarse-grained to reduce a large amount of unnecessary data. This coarse-graining is done in two steps. First, position data is rounded to the nearest millimeter. Then after computing S, the average speed over every 25 successive time steps yields a temporal resolution of 0.25 seconds. Once coarse graining is complete, the bead speed average is calculated by averaging the speed of all eight beads across a single time bin.

A second, binary velocity vector will also be used throughout analysis and is computed using the mean bead speed throughout the recording (after coarse-graining). If the bead speed of the time bin is above the mean bead speed for the recording, that time bin is set to 1, otherwise it is set to 0. The mean bead speed for any given recording is very close to zero making this binary vector highly representative of actual periods of motion and rest.

A similar process of temporal graining is carried out with the raw spiking data. After the unique unit and accompanying spike times array is imported, a spike count time series is computed with a temporal resolution of 0.25 seconds. First, a time vector of consecutive 250ms time bins is created which spans the length of the recording. Then, using the Matlab ‘histc’ function (which counts entries of a vector which fall within pre-specified bins) a spike count vector is produced. The spike count vectors for each unique neuron are placed into a matrix leaving an NxM array (N unique units, M time bins) with spiking data for the recording.

Along with the binary velocity vector, a binary spike array will also be used later in analysis. The computation is analogous to the binary velocity vector in that if the spikecount of a neuron within a time bin is above its mean value throughout the recording, the time bin is set to 1, 0 otherwise.

The method by which recordings were synced during recordings was through simultaneous mouse-clicks on both recording stations. While this method time locks the two

recordings, it does not produce recordings of the same length. The following analysis will require arrays of similar lengths, therefore the longer of the two arrays (post coarse-graining) is determined and the shortened to match the shorter array.

Behavior activity

Cumulative distance traveled, that is, the total distance traveled throughout individual recordings was chosen to quantify the animal's overall behavior and is computed by,

$$D = \sum_{i=0}^{N} v_i(0.01s)$$

where v_i is the mean bead velocity of the i^{th} timestep which, when multiplied by the timestep length (0.01s), gives distance traveled during the i^{th} timestep. By assigning a single value to individual recordings, tracking behavior changes due to inhibitory modulation is determined by increases or decreases in total distance traveled.

Population coupling

Population coupling is a measure of how strongly the activity of a single neuron is related- or coupled to the activity of the network in which it is embedded. The method we chose to quantify population coupling was introduced in a previous study[2]

$$c_i = \frac{1}{|f_i|} \sum_t f_i(t) \sum_{j \neq i} (f_j(t) - \mu_j)$$

where $|f_i|$ is the total spike count of neuron i through the recording, $f_i(t)$ and $f_j(t)$ are the spike counts of neuron i and j respectively in time window t, and μ_j is the time averaged spike count of neuron j. A single value of population coupling is obtained for each neuron in a recording.

Population coupling quantifies the relationship between the firing of individual neurons and the firing rate of the population, therefore the question of why this new method of population

coupling is used as opposed to other, more standard practices in computing the correlation between two variables (e.g. Pearson correlation coefficient, etc.) naturally arises. Standard correlation coefficient values have been shown (Okun et al. 2015; De La Rocha et al. 2007; Dorn 2002) to be biased toward neurons with higher spike rates (higher firing rates lead to higher correlation coefficients) whereas population coupling is invariant to individual neuron- and population firing rates.

Body coupling

Body coupling is a measure of how strongly the activity of a neuron is correlated to the activity of the movement of the animal's body throughout a recording. This quantity is calculated in two different ways.

The first method is through a calculation of the mutual information between specific body movements and spiking data of a single neuron centered around said body movements. However, several arbitrary decisions (choice of coarseness of recordings, average velocity thresholding for binary velocity matrix) are made which, when adjusted, lead to changes in individual values as well as the relationship between those values. While this method of calculating body coupling works in theory, application to limited, real world data sets could lead to several issues which are outlined below. Although mutual information analysis was eventually abandoned, the concept laid the foundation of future analysis techniques and is therefore included. Subsequently, the first method of determining a neuron's body coupling is by way of movement-triggered-average spike rate (MTASR) waveforms. Along with the MTASR method of body coupling a second, similar approach was created which uses spike-triggered average body speed (STABS) waveforms.

Mutual information

Mutual information, a quantity which describes the mutual dependence between two variables, is defined as

$$I(X;Y) = H(X) - H(X|Y)$$

where $H(X)$ is the entropy contained in the variable X and $H(X|Y)$ is the conditional entropy between X and Y. Given the probabilities and relationship between the two variables, these entropies can be calculated as follows:

$$H(X) = -\sum_{i=1}^{n} P(x_i) \log_2 P(x_i)$$

where $P(x_i)$ is the probability of state x_i and

$$H(X|Y) = -\sum_{i,j} P(x_i, y_j) \log_2 \frac{P(x_i, y_j)}{P(y_j)}$$

where $P(x_i, y_j)$ is the probability that $X = x_i$ and $Y = y_j$. The quantity $P(x_i, y_j)$ can be thought to represent the randomness in variable Y given event X. A base of 2 in the logarithm gives entropies and information in units of bits. Any base can be used (without affecting results) but the choice of 2 is standard when dealing with information calculations.

X is a two-state variable related to the motion of the body and is defined as either movement onset or cessation. These states are determined from the binary velocity vector as transitions from 0 to 1 (onset) or 1 to 0 (cessation). The states of the Y variable are 4-bin (1 second) binary spike vectors centered, or triggered, on times of movement onsets and cessations. After computing the corresponding probabilities of each state (in the usual way), entropy, mutual entropy, and finally mutual information are calculated.

Significance of calculated I values was tested by constructing 100 surrogate spike matrices (with randomly shuffled spike times) and I was recomputed with the movement triggers

and these surrogate spike matrices. Neurons were deemed significant if actual I values were greater than 90% of surrogate values.

While this measure of body coupling is sufficient as a theoretical definition, in practice two problems arise, (1) due to the finite nature of our data sets and the use of probabilities within the mutual information calculation, under-sampling might lead to somewhat skewed results and (2) the 0.25 s time binning and subsequent binarization of spike data reduces the amount of useful information obtained during recordings (e.g. raw spike counts and times). Therefore, we created a new measure of body coupling which uses total spike count waveforms centered on movement initiation or cessation times (movement-triggered-average spike rate (MTASR)).

MTASR

This method of body coupling analysis begins with the movement initiation and cessation triggers obtained previously as well as the raw spike time files collected via spike sorting algorithms. First, for each movement trigger time, spikes for a single neuron are collected into 20 0.1 s time bins centered around the trigger (1 second before and 1 second after the trigger). Second, all spike counts are divided by bin width (0.1 s) to give the spike rate. Next, the average is taken over all movement initiation or cessation triggers to obtain an average spike rate waveform which displays the activity of a single neuron with respect to certain animal actions (movement initiation or cessation). Finally, the body coupling value for a neuron during movement initiation or cessation (two values of body coupling per neuron) is computed as the standard deviation of these average waveforms,

$$\sigma = \sqrt{\frac{\sum_i (x_i - \bar{x})^2}{(n-1)}}$$

where x_i is the spike rate of the ith time bin, $\bar{x}$ is the average spike rate over all bins, and n is the number of bins, in this case 20. A greater change in spiking activity (whether an increase or decrease in spike rate) with respect to the animal's behavior translates to a larger standard deviation, and therefore a larger value of body coupling.

To test for significance, body coupling was computed using surrogate MTASR waveforms created using randomly shuffled spike times relative to body movement times (100 surrogates per actual MTASR waveform). Waveforms were deemed significant if actual body coupling values were greater than 95% of surrogate values.

STABS

Beginning from raw spike times and the spatial-grained average body speed vector, the spike-triggered average body speed waveform is computed by extracting 2-second body speed waveforms centered on spike times of a neuron. Averaging over all triggers for an individual neuron results in a single waveform which is representative of the animal's average behavior both 1 second before, and 1 second after spike events.

Again, the value of body coupling is computed as the standard deviation of the STABS waveform,

$$\sigma = \sqrt{\frac{\sum_i (x_i - \bar{x})^2}{(n-1)}}$$

where x_i is a point in the waveform, $\bar{x}$ is the average value, and n is the number of points (200 for a recording rate of 100 Hz). A waveform with high variability represents a neuron which is consistently correlated with a specific change in body speed whereas a waveform which is relatively flat could represent a neuron which fires independently of changes in body speed.

Results

In this experiment we conducted simultaneous recordings of behavior and single unit spiking activity of unconstrained adult male rats. 3-dimensional behavior data was obtained via an infra-red (IR) camera motion capture system (OptiTrack) in conjunction with eight 3mm reflective beads placed along the animal's back side and hind limbs. Extracellular neural recordings were obtained via chronically implanted 32-channel micro-electrode arrays spanning deep layers (V/VI) of primary motor cortex. Electrode orientation (perpendicular to dorsal surface, parallel to midline) and position (0.5 mm caudal from bregma, 2 mm lateral from bregma, and spanning 1.4 mm in the rostrocaudal direction) were deliberately chosen based on previous intracortical microstimulation studies within primary motor cortex (Kolb 1990). This area is responsible for a large number of body movements including hip flexion, trunk movements, pronation, wrist extension, elbow flexion, neck movement, and vibrissa movement. Single unit spiking activity was extracted via spike sorting software (OfflineSorter, Plexon) using conventional principle component analysis techniques.

Global inhibitory modulation

A total of 732 individual spiking units (367 no drug, 193 PTZ, and 172 muscimol) were obtained from 73 30-minute recordings (36 no drug, 19 PTZ, 18 muscimol, n=3 rats). Drugs were administered via intraperitoneal injection with a consistent dosage across all recordings (2mg/kg bodyweight for both PTZ and muscimol) at a volume of 1ml/kg bodyweight. A 1mL/kg bodyweight volume was maintained throughout saline sham injections.

Behavior

As an initial test of pharmacological manipulation, overall behavior was quantified using cumulative distance traveled throughout recordings. The saline sham control recordings

exhibited a median cumulative distance traveled of 3.92 meters. This median distance increased to 11.82 meters for global PTZ application and decreased to 2.02 meters for global muscimol application. Thus, decreased synaptic inhibition tended to result in more body movement (p=0) of the animals, while increased synaptic inhibition had the opposite effect (p=0).

Spiking activity

As a first look at how inhibitory modulation alters neural activity in motor cortex we examined the spike rate and variability of firing (CV ISI) for each neuron. Spike rate and CV ISI versus drug condition are shown in figures 9 and 10 respectively. Spike rate across neurons remains relatively unchanged from sham recordings to global inhibitory modulation cases (p=0.38 PTZ, p=0.05 muscimol). There is a slightly wider range of spike rates for global PTZ application, but this increase in variability insignificant. Similarly, CV ISI tends display similar mean and quartile values across drug conditions (p=0.13 PTZ, p=0.06 muscimol). Thus, even though body movement exhibited substantial changes due to modulation of inhibition, spike rate and CV ISI did not. This raises the question; which aspects of neural activity do change due to these changes in inhibition. In the next section, we show that one answer to this question is the degree of coordination among neurons to the network activity, which we quantify using 'population coupling'.

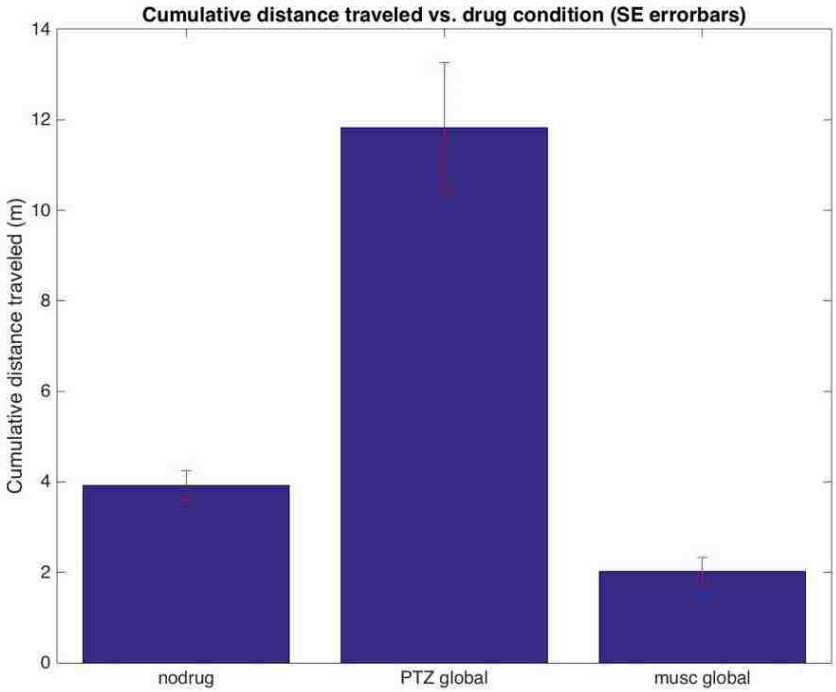

Figure 8 – Cumulative distance traveled vs. drug condition for global inhibitory modulation. Altering inhibition globally leads to large changes in cumulative distance traveled for both drug cases. Bars represent average data over all rats and all recordings for a given drug condition. Error bars represent standard error over all drug-specific recordings.

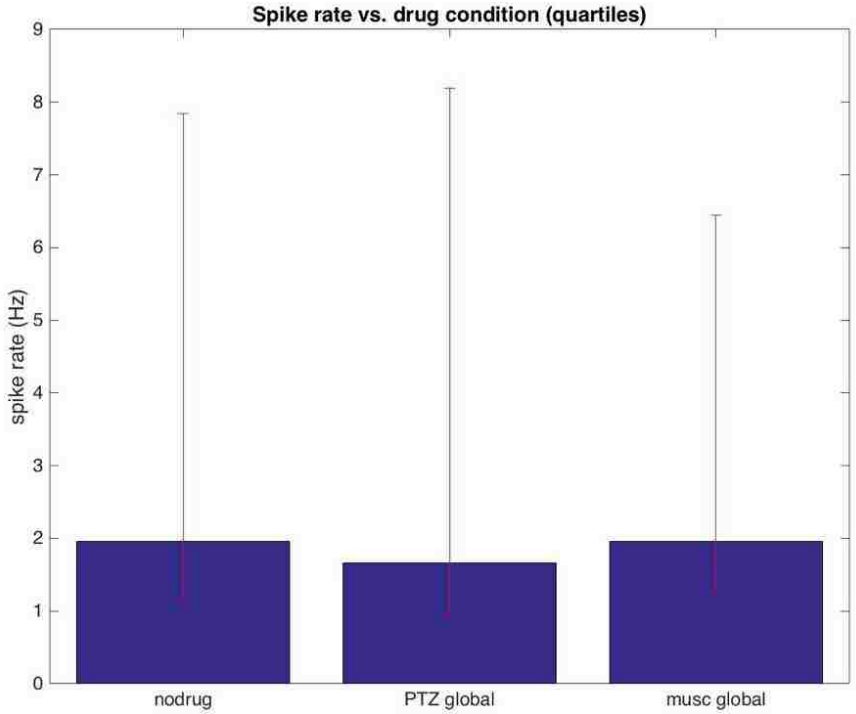

Figure 9 – Spike rate vs. drug condition for global inhibitory modulation. Neuron spike rates remain relatively unchanged across drug conditions. Blue bars represent average spike rate values over many neurons for each drug condition. Error bars display first and third quartiles for data taken from many neurons.

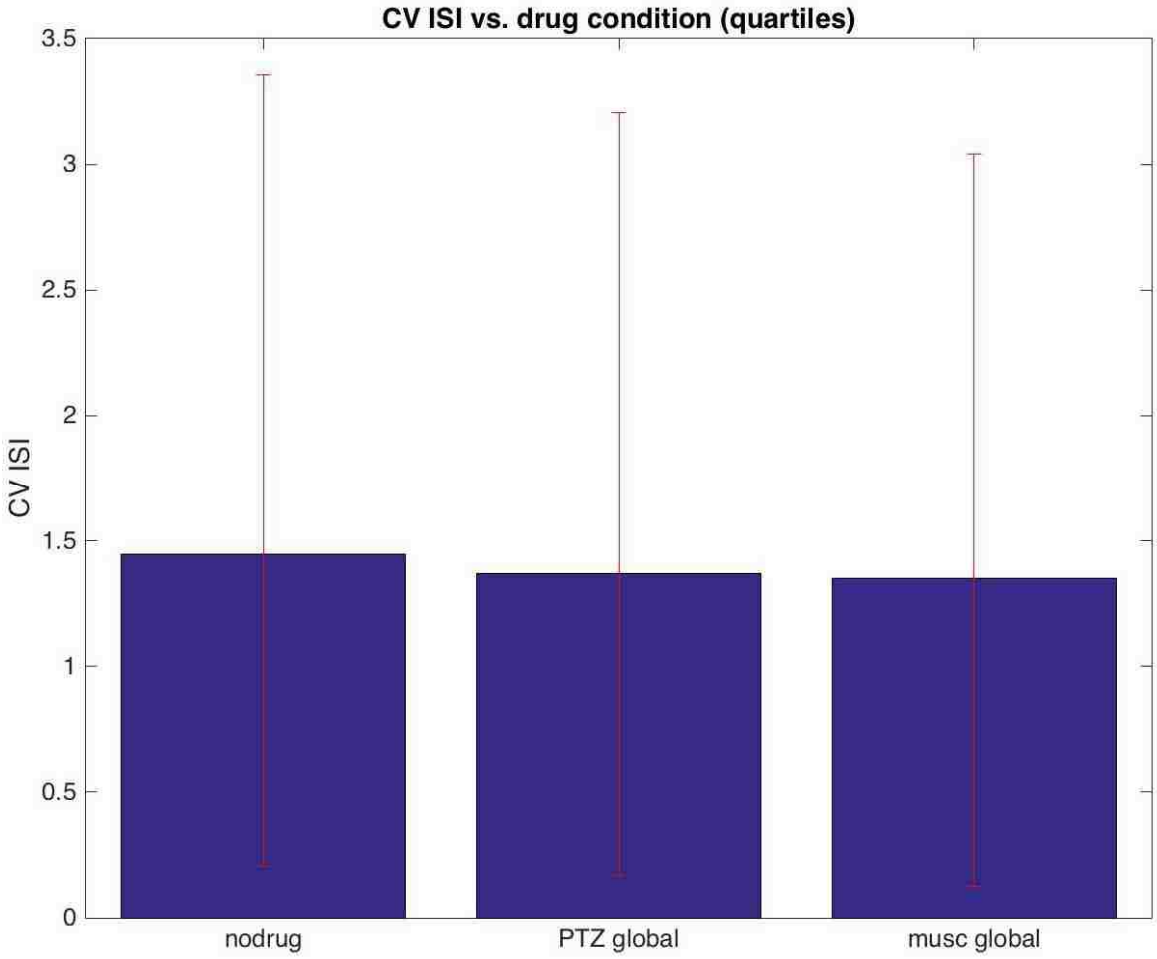

Figure 10 – CV ISI vs. drug condition for global inhibitory modulation. Similar to spike rates, CV ISI values are largely unaffected by global changes in inhibition. Height of blue bars represents average CV ISI value over many neurons. Error bars represent first and third quartiles of data taken from many neurons.

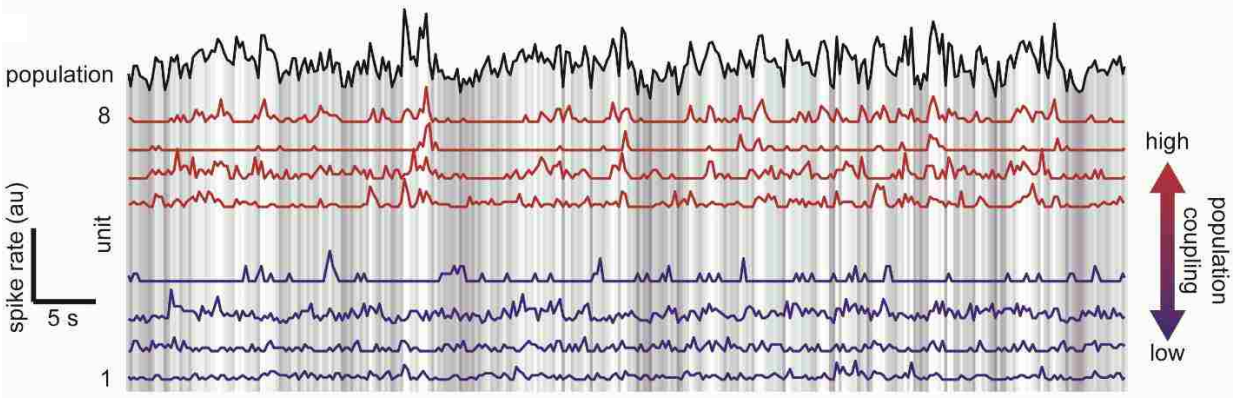

Figure 11 – Sample population coupling time series. Solid black line and gray scale represent summed population spike activity. Red and blue lines represent spike count time series of single neurons with high and low values of population coupling respectively. Population coupling displayed a high degree of variability across neurons within a recording as well as across individual recordings.

Population coupling

Population coupling (Okun et al. 2015), a variable which quantifies the similarity of a single neuron's activity to the summed activity of the whole population in which it is embedded, was computed using spike count time series. Spike count time series were determined by first discretizing recordings into 0.25-second time bins, then counting spikes for individual neurons in each time bin. Next, the spike count activity of a single neuron was compared to the summed spiking activity of the remaining neurons in the recording to determine its population coupling strength. Neurons which co-varied more with the population were said to have a high value of population coupling whereas those which did not exhibit a strong correlation are defined as having a low value of population coupling. Population coupling exhibited a wide range of values across not only separate recordings, but between individual neurons within the same recording as well. Figure 12 shows median population coupling versus drug condition (error bars represent standard error in data). Whereas population coupling was largely unaffected by application of PTZ ($p=0.05$), there is a significant increase in population coupling across global muscimol recordings ($p=0$). Thus, although enhanced inhibition did not change the firing rates or the variability of firing (CV ISI), it did cause a large increase in population coupling.

Previously (Okun et al. 2015), population coupling was studied in sensory cortex and shown to be nearly unchanged when comparing periods with and without sensory stimulation. This suggests that the population coupling of a neuron is a property which is independent of whether the neuron is engaged in the outside world or not. To test this hypothesis in our data, population coupling values were computed during periods of motion and rest (motion and rest defined as times when average bead speed is above- or below time averaged mean bead speed respectively). If population coupling is indeed independent of whether the neuron is engaged in the outside world or not, then population coupling should remain constant irrespective of motor output.

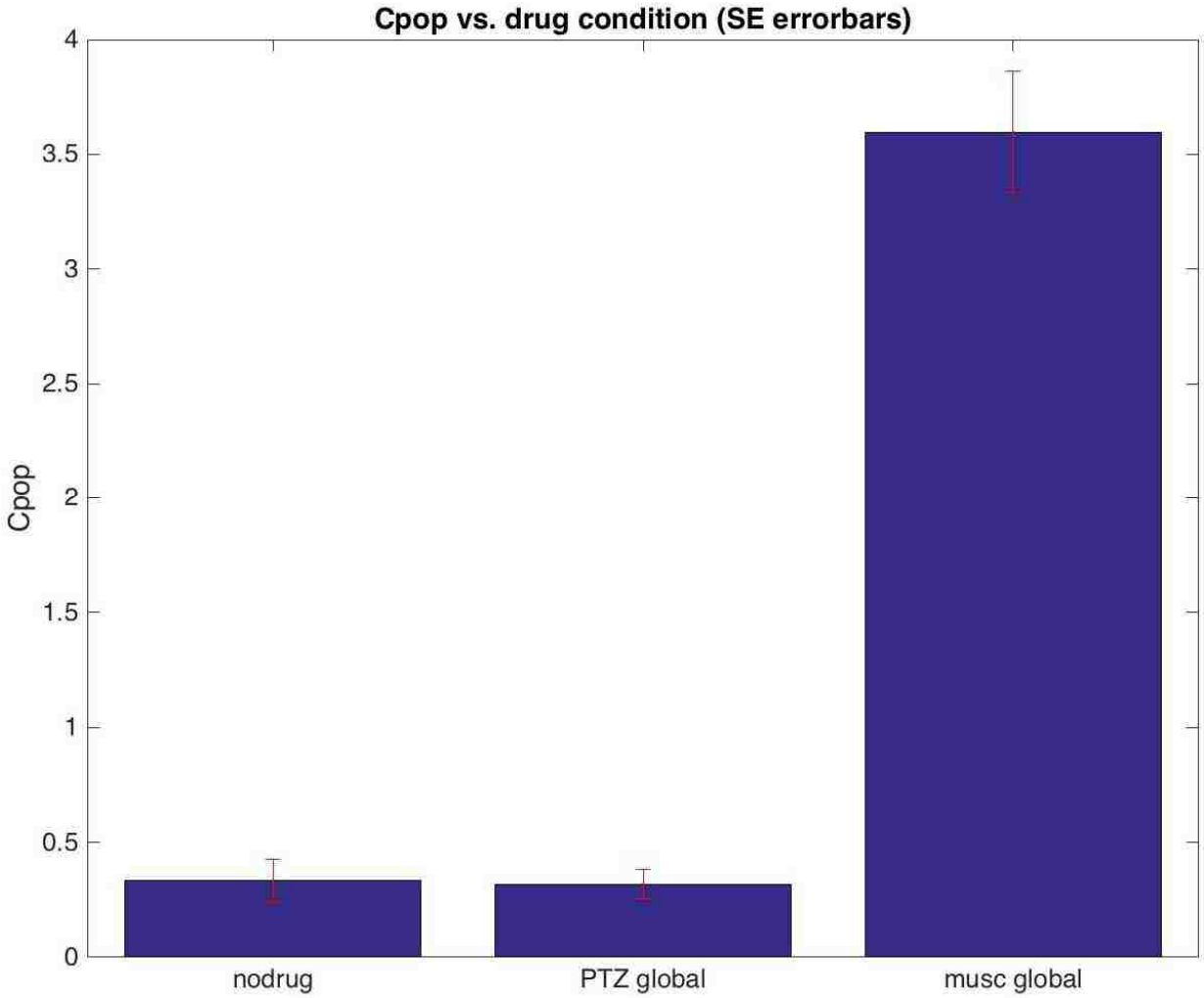

Figure 12 – Population coupling values averaged over many neurons for global changes in inhibition. Population coupling was largely unaffected when inhibition was decreased globally (PTZ). However, increased inhibition (muscimol) led to large increases in population coupling values. Height of blue bars represents the mean over many neurons. Error bars represent standard error over many neurons.

Our data shows a strong trend for similar values of population coupling during periods of motion and rest (solid line represents unity). However, population coupling tends to increase during periods of rest for muscimol recordings.

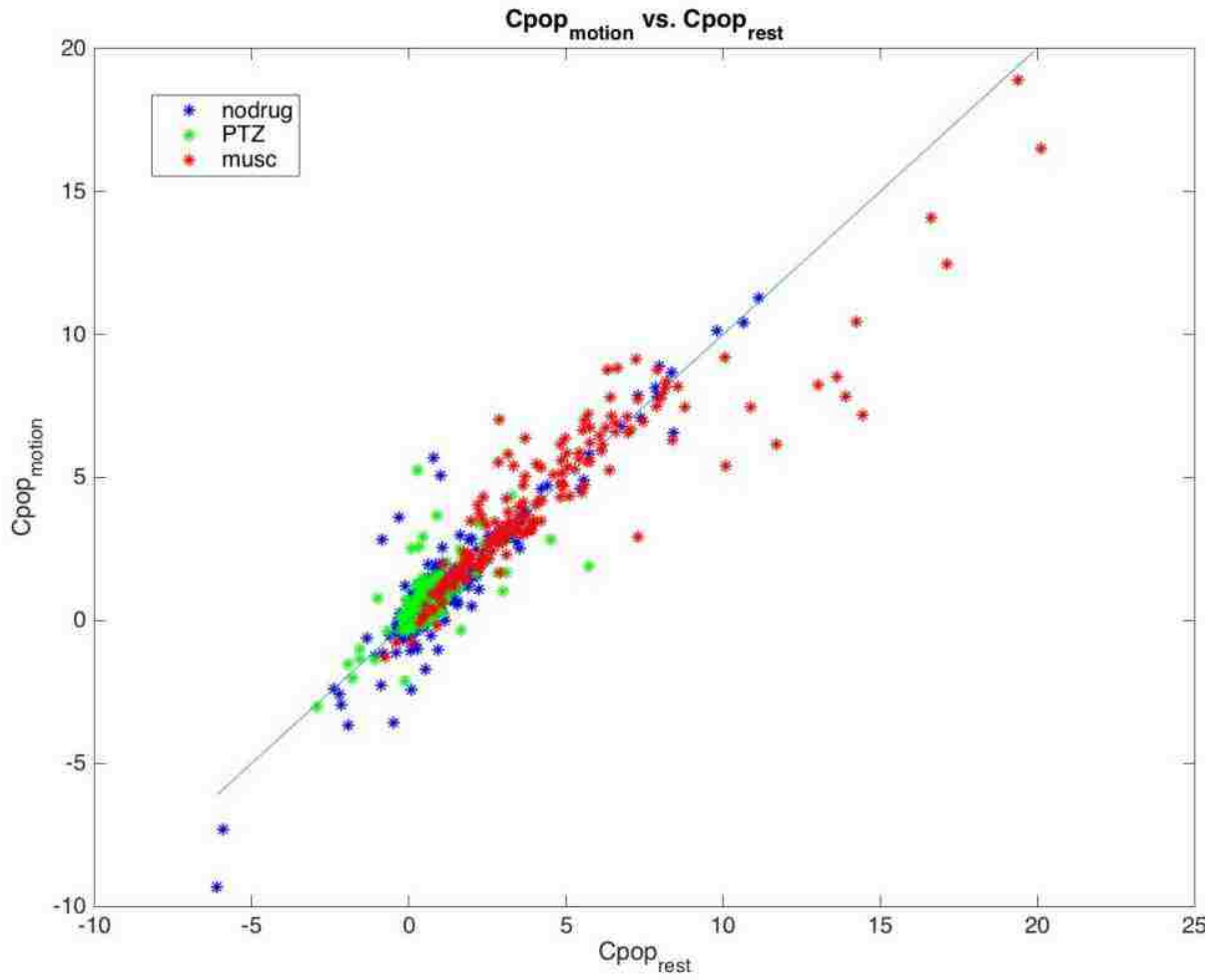

Figure 13 - Population coupling during periods of motion vs. periods of rest for global inhibitory modulation. Each point in this plot represents one neuron. Population coupling for individual neurons tends to remain constant throughout changes in behavior (solid line represents unity). However, several neurons with higher values of population coupling tended to deviate from unity during application of muscimol.

Local inhibitory modulation

The global modulation of inhibition discussed above has several advantages. For instance, medications that act on inhibition act globally. To better understand the mechanisms and neural correlates of such medications, experiments like our global manipulations can be important. However, it is difficult to interpret precisely what is responsible for the observed changes, because global manipulations act at many different parts of the nervous system (not just in the cortex). To get a better understanding of how much of the results from last section are due to local changes in motor cortex we did another set of experiments in which we applied the drug locally in motor cortex.

A total of 952 individual spiking units (477 no drug, 255 bicuculline, and 220 muscimol) were obtained from 155 30-minute recordings (82 no drug, 38 bicuculline, 35 muscimol, n=3 rats). Increasing concentrations of bicuculline and muscimol were applied by repeatedly doubling the solution concentration (from 20-640 μM). Infusions were administered at 0.2 μL/min over either 5 or 10 minutes (resulting in 1 μL and 2 μL volumes). Total infused molarity was chosen when labeling drug concentrations (e.g. a 640 μM concentration administered at 0.2 μL/min over 10 minutes resulted in a 1280 μM dose).

Behavior

Behavioral response to local pharmacological manipulation was not as drastic when compared to global manipulation of inhibition. Figure 14 shows the median distance covered versus drug condition. Although there is a sharp spike in observed movement for high concentrations of bicuculline administration, there is not a significant trend across concentrations (ρ=0.18, p=0.22). Contrary to these results, there is a significant trend through application of muscimol where movement increased with increasing concentration (ρ=0.49, p=0.003).

Spiking activity

Unlike with the experiments using global manipulations of inhibition, we found that spike rates tended decrease with increasing concentration of muscimol (ρ=-0.15, p=0.02). However the change was insignificant for increasing concentrations of bicuculline (ρ=0.06, p=0.35). The change in spike rates (figure 15) for local decreases in inhibition agree with previous findings (Bader et al. 2017)[Bader]. Similar to global changes in inhibition, CV ISI was invariant to local decreases (ρ=0.02 , p=0.7) and increases (ρ=0.05 , p=0.48) in inhibition (figure 16).

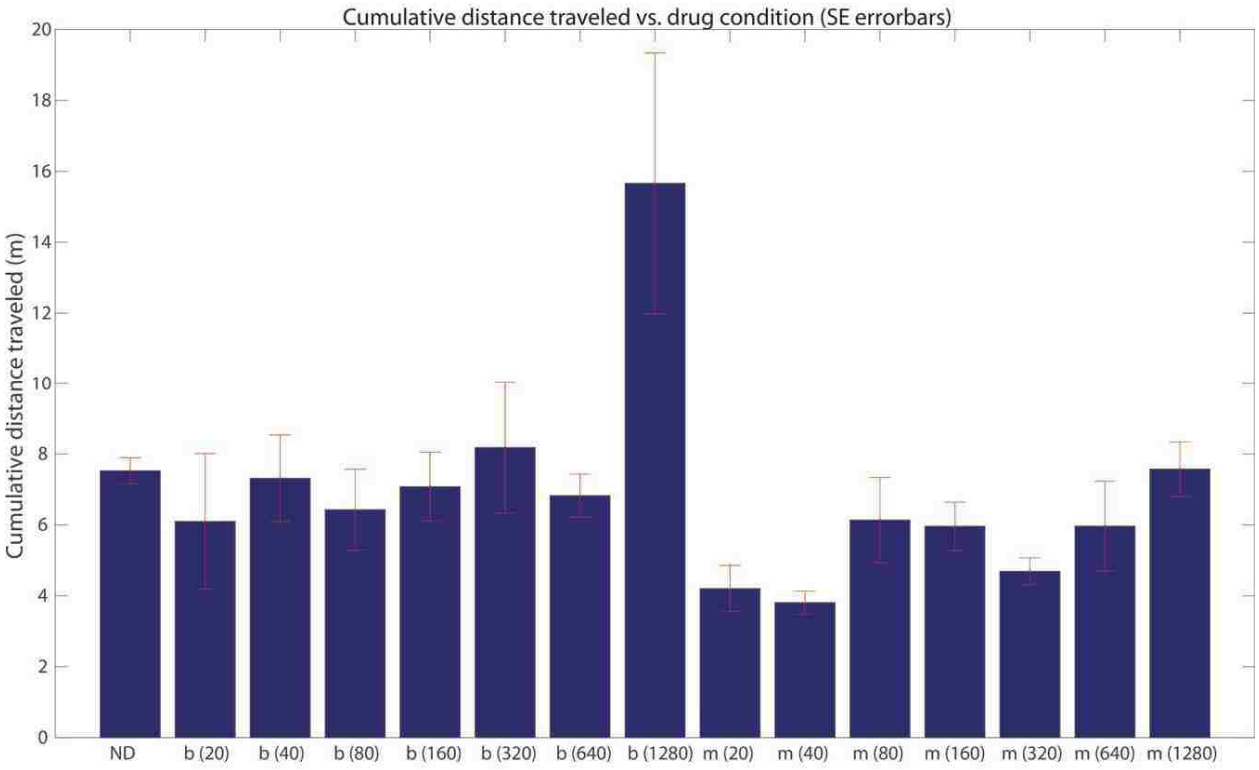

Figure 14 – Cumulative distance traveled during a 30-minute period versus drug condition (ND=no drug, b=bicuculline, m=muscimol) for local inhibitory modulation. Aside from the drastic increase for high bicuculline concentration, distance traveled remains relatively constant across drug conditions. Blue bars represent average over recordings for specific drug and concentration. Error bars represent standard error within data. Drug concentrations in μM

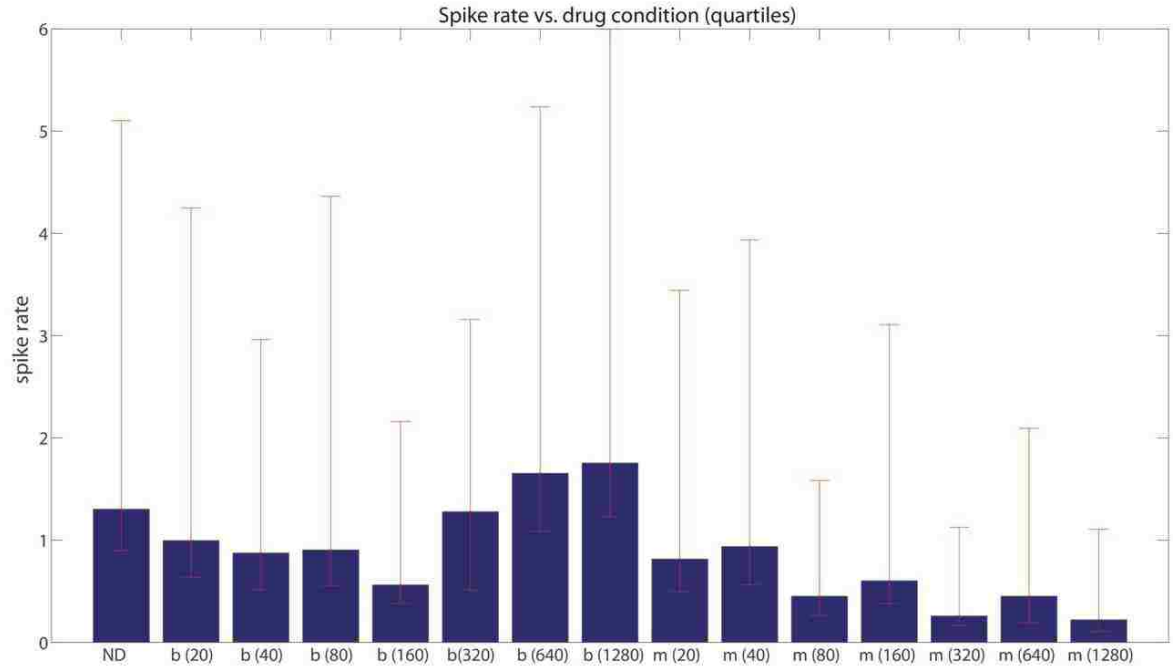

Figure 15 – Spike rate versus drug concentration (ND=no drug, b=bicuculline, m=muscimol). An inverse relationship exists between spike rate and local changes in inhibition, i.e. when inhibition is increased, spike rate decreased and vice versa. Blue bars represent average over many neurons for specific drug and concentration. Error bars represent first and third quartiles within data. Drug concentrations in μM

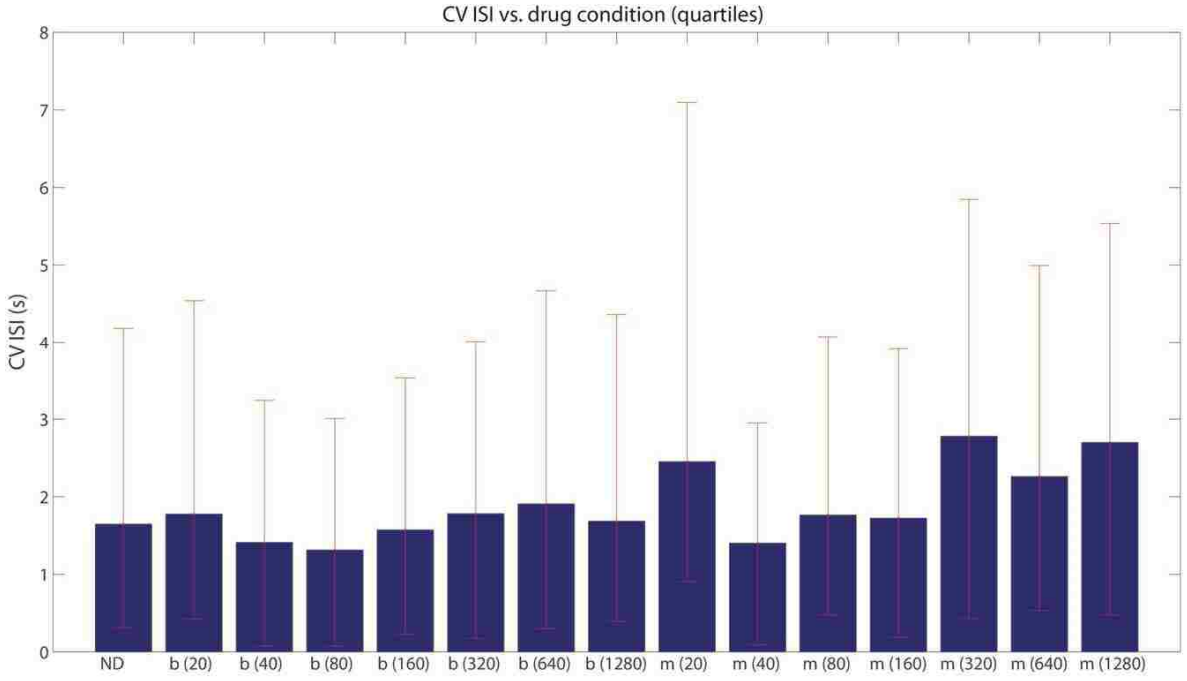

Figure 16 – CV ISI versus drug concentration (ND=no drug, b=bicuculline, m=muscimol). CV ISI was largely unaffected by local decreases in inhibition whereas there was a slight increase during increased inhibition cases. Blue bars represent average over many neurons for specific drug and concentration. Error bars represent first and third quartiles within data. Drug concentrations in μM.

Population coupling

Whereas population coupling was largely unaffected by global application of PTZ, decreasing inhibition locally via bicuculline resulted in higher values of population coupling in cortex (ρ=0.15 , p=0.02) (Figure 17). Similar to global increases in inhibition, there was a consistent rise in population coupling with increasing concentration in local application of muscimol (ρ=0.31 , p=0).

Figure 18 shows population coupling for periods of motion versus periods of rest for single neurons. There is a strong trend for similar values of population coupling during periods of motion and rest (solid line represents unity).

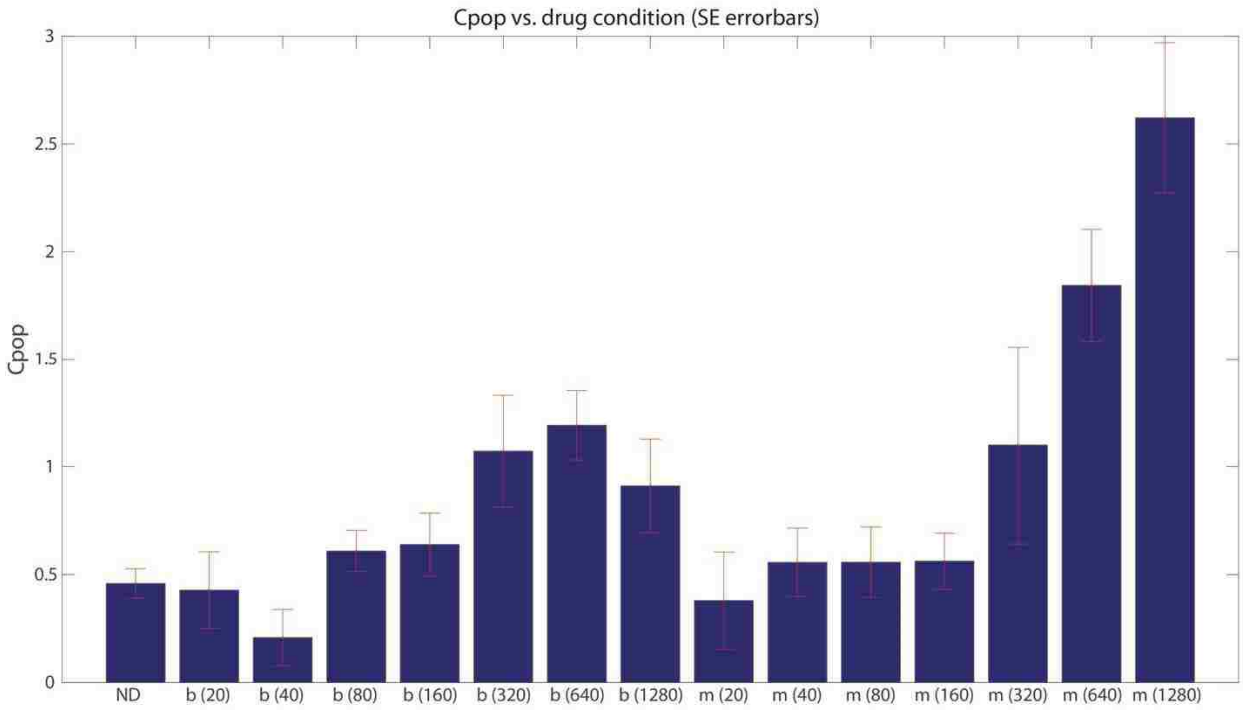

Figure 17 – Population coupling versus drug concentration (ND=no drug, b=bicuculline, m=muscimol). Population coupling increased for both increased and decreased local inhibition. Higher concentrations of muscimol displayed the largest increase in population coupling. Drug concentrations in μM

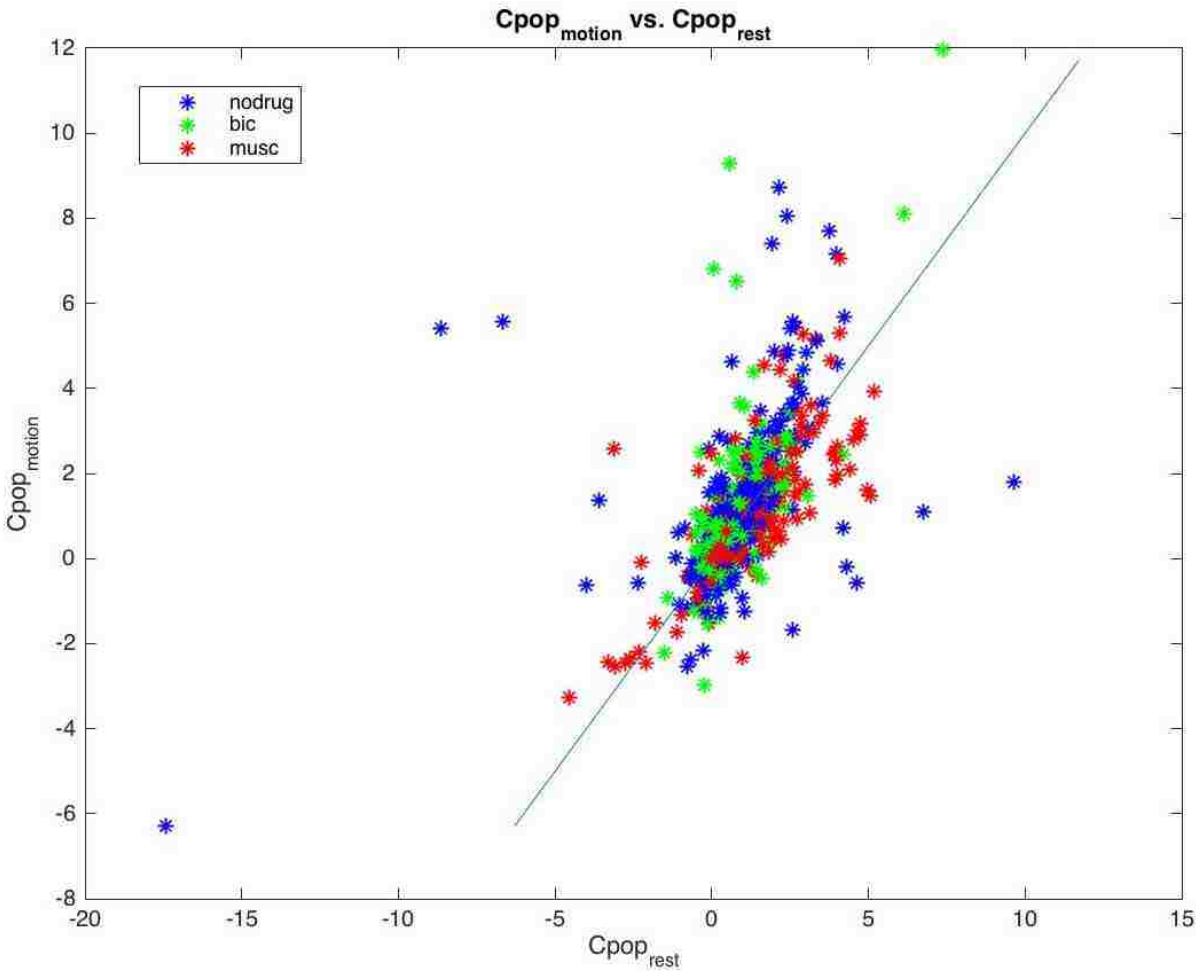

Figure 18 – Population coupling during periods of motion versus periods of rest for local inhibitory changes. Population coupling for individual neurons tends to remain constant throughout changes in behavior. Each point represents an individual neuron (color indicates drug condition). Line represents unity.

Body coupling

Neuron-to-body coupling was computed using two distinct methods. The first method uses movement-triggered-average spike rates (MTASR), wherein spikes were counted within a 2-second time window (40 time bins, each 0.05 s in duration) centered on velocity events (triggers). Two types of velocity trigger events were considered: movement onset or cessation times (defined as times when the average bead speed rose above or dropped below the time-averaged mean bead speed respectively). Averaging over all onset and cessation triggers separately results in two 2-second average spike rate waveforms corresponding to the average activity of a single neuron around the times of body movement initiations or cessations. To quantify how much a neuron's spike rate was modulated with body movement we computed the standard deviation (across time) of the MTASR waveform and refer to this quantity as body coupling (BC_M). A flat line MTASR would indicate a neuron that fires independently of body movement (zero standard deviation). Higher standard deviation, i.e. high body coupling, implies that the neuron's spike tends to change when the animal moves (or stops moving).

In computing body coupling via the MTASR method several arbitrary choices of parameters were made (time bin durations, speed threshold value to define movement onset and cessation, etc.). Our results were robust to some variation in these parameter choices, but nonetheless, to better support our findings, body coupling was computed via a second method. This method is based on the spike-triggered-average body speed (STABS) waveform. A STABS waveform is the average of all 2-second raw body speed waveforms centered on spike times (triggers) of an individual neuron. Similar to how body coupling was defined based on the MTASR calculation, we computed standard deviation (across time) of the STABS waveform to quantify body coupling (BC_S). A small standard deviation would imply that a neuron fires independently of body movement and a larger standard deviation implies the spike times of a neuron are associated with body movement.

Movement triggered average spike rate (MTASR)

Initially, MTASR waveforms are low-pass filtered with a cutoff frequency of 4 Hz and normalized by their mean value. MTASR body coupling (BC_M) values are deemed significant if their value is greater than 95 of 100 surrogate values (surrogate waveforms are created by randomly shifting spike times relative to movement triggers and recomputing MTASRs). Across all drug conditions, approximately 30% of neurons were shown to have strong significance. Similar to population coupling (C_{pop}), BC_M values exhibited a broad range of values across all drug conditions. Figure 20 shows BC_M versus C_{pop} for individual neurons throughout all experiments.

The primary finding of our work is that the relationship between body coupling and population coupling exhibits a peak (Figures 20 & 23). Neurons that were most engaged with the other neurons in cortex (i.e. those with highest population coupling) were mostly unrelated to body movement (i.e. had low body coupling). Similarly, for very low population coupling, body coupling was low. Neurons with an intermediate value of population coupling exhibited the highest body coupling.

The simplest way to see the peaked relationship between body coupling and population coupling is to compute a 'moving average' of body coupling along the population coupling axis (dark line in Figure 20). However, we also did more quantitative tests of statistical significance of this relationship by computing correlations between body coupling and population coupling. We computed the correlation on the rising side of the peak (expecting significant positive correlation) and on the falling side of the peak (expecting significant negative correlation). Calculation of Spearman's rank correlation coefficient ρ for BC_M vs C_{pop} was performed for values less than- or greater than BC_M peak values (normal inhibition rising side $C_{pop}<0.5$, $\rho=0.127$, $p=0.008$; normal inhibition falling side $C_{pop}>0.45$, $\rho=-0.117$, $p=0.017$; reduced inhibition rising side $C_{pop}<0.6$, $\rho=0.187$, $p=0.03$; reduced inhibition falling side $C_{pop}>0.4$, $\rho=$-

0.167, p=0.040; enhanced inhibition rising side C_{pop}<5, ρ=0.228, p=0.005; enhanced inhibition falling side C_{pop}>4, ρ=-0.262, p=0.009). Here the p values represent the probability of the null hypothesis that the values are uncorrelated, computed based on many surrogate data sets in which the order of body coupling and population coupling values are randomly shuffled.

Some neurons were excluded from our analysis due to two important factors. First, in order to analyze our results when inhibition was clearly affected, we excluded recordings with low local drug concentrations, which had little to no effect on population coupling. To determine the 'cut-off' concentration, we used C_{pop} values as a guide (figure 17). It is clear that for both muscimol and bicuculline concentrations under 320 μM, C_{pop} values are similar to no drug values. Therefore, neurons from recordings with drug concentrations of 160 μM and below are excluded from analysis. Second, neurons with extremely low spike rates (<150 spikes/recording) were also excluded as using the spiking activity from these neurons can lead to MTASR and STABS waveforms with misleading body coupling values.

Spike triggered average body speed (STABS)

Figure 21 shows an example of a STABS waveform with relatively high body coupling (indicative of the sharp peak around t=0). Waveforms were low pass filtered at 4 Hz and normalized by their mean between -1.0 to -0.75s with respect to the trigger time. One hundred surrogate waveforms were computed for each neuron by temporally shifting body data (surrogate number*1/100th of total recording time) and re-computing the waveform (gray lines in figure 21).

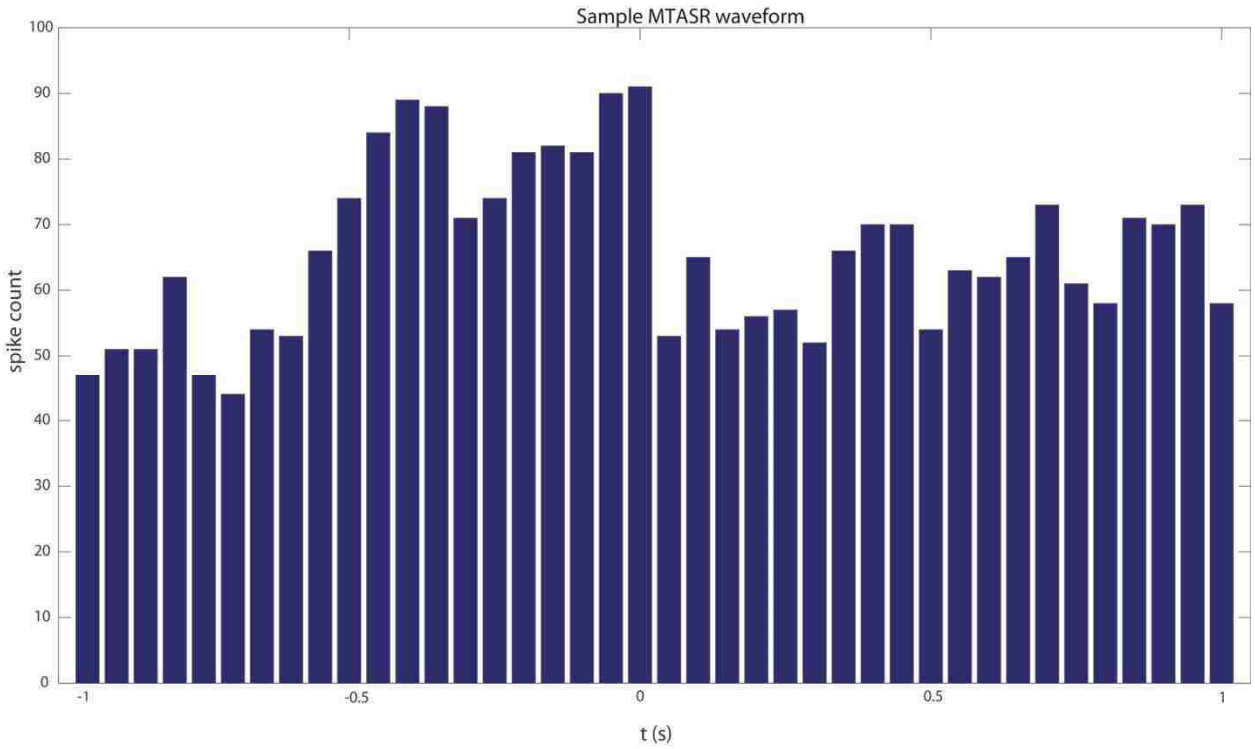

Figure 19 - Sample MTASR waveform. Waveforms consist of 40x0.05 s bins (2-second window centered on triggers) of average spiking activity for a single neuron summed over all movement initiation or cessation triggers. This particular neuron tended to increase its spiking activity in preparation for movement initiation (t=0). All combinations of increased, decreased, and unchanged spiking activity were seen for both movement onset and cessation triggers.

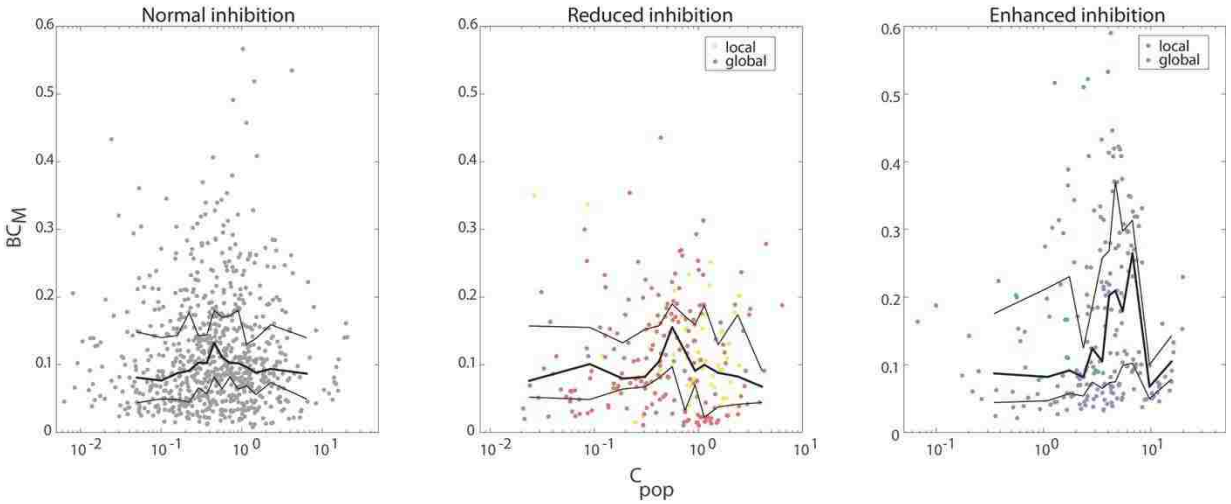

Figure 20 - Body coupling (computed using MTASR method (BC_M)) versus population coupling (C_{pop}). Plots indicate inhibitory modulation condition. Points represent individual neurons from single recordings, BC_M values Z-scored for significance. Thick black line indicates moving average over all points while thin lines indicate first and third quartiles of data. BC_M exhibits a peak near low values of C_{pop} and decreases with increasing or decreasing C_{pop}.

A similar peaked relationship between body coupling and population coupling is seen when body coupling is computed using the STABS method. Figure 23 shows body coupling versus population coupling for normal, decreased, and increased inhibition cases.

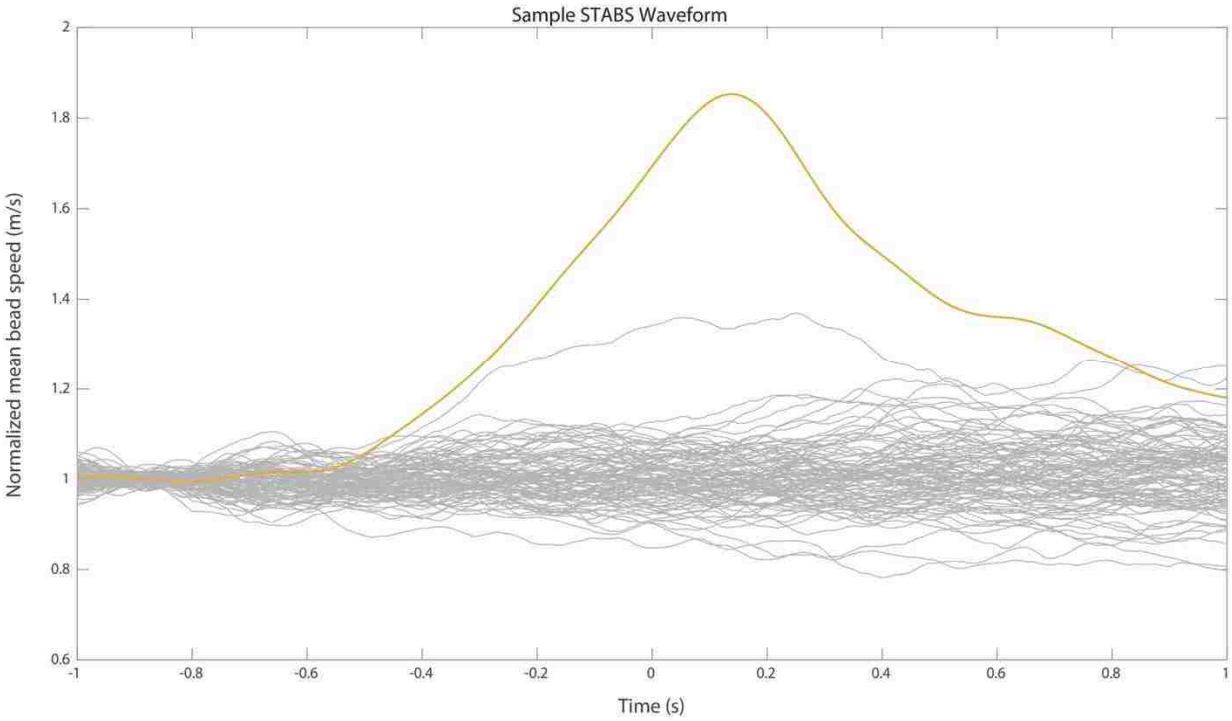

Figure 21 - Sample STABS waveform. Neurons with higher values of body coupling exhibit larger deviations in their STABS waveforms. Actual STABS waveform shown in yellow, 100 temporally-shifted surrogate waveforms shown in gray.

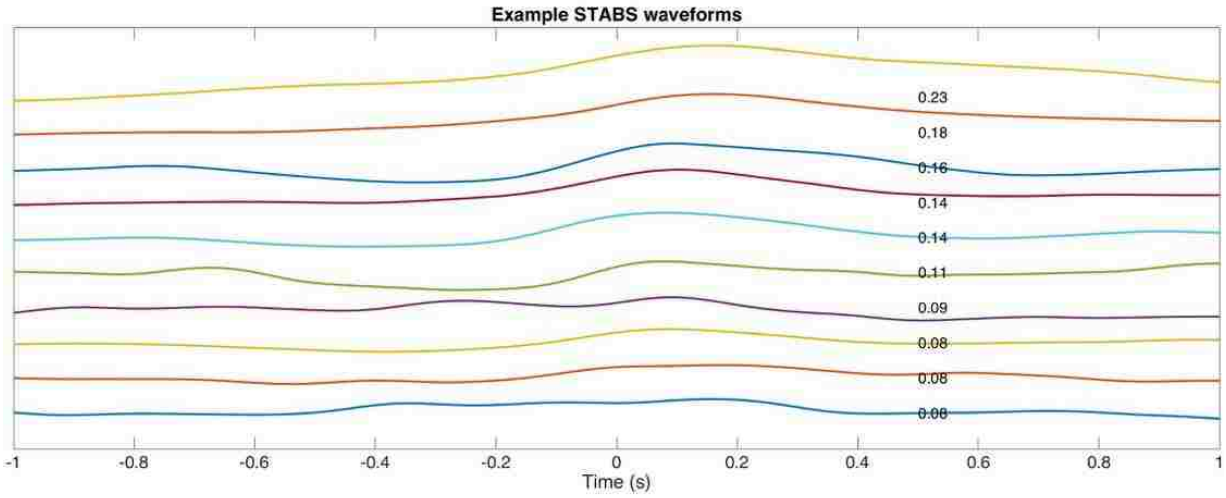

Figure 22 - Example STABS waveforms and their respective body coupling values. Body coupling values are computed as the standard deviation of the STABS waveform. As seen in the figure, larger fluctuations of the waveform lead to higher body coupling values.

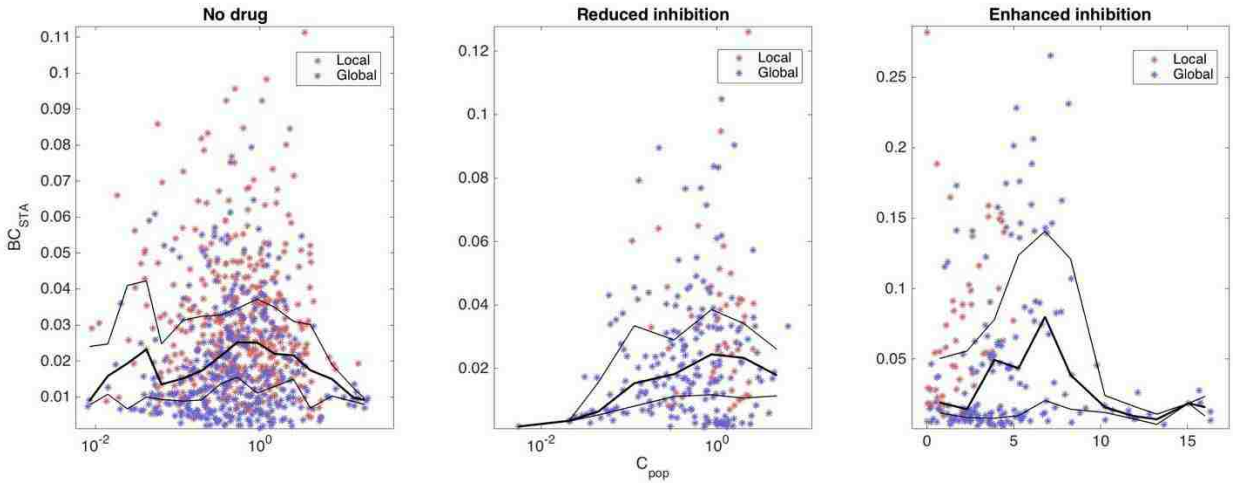

Figure 23 –STABS computed body coupling versus population coupling for individual neurons. An inverse relationship exists between population coupling and body coupling. Thick and thin black lines represent median and quartile values respectively.

Conclusions and Discussion

The coordinated interactions of large groups of neurons within cortex and lower-level brain structures produce our experience of- and interactions with the outside world. It has been shown that the spiking activity of a population of neurons can be either synchronous or asynchronous and thus has been a topic of debate for decades (Gray and Singer 1989; Womelsdorf et al. 2007; Canolty et al. 2010; Markopoulos et al. 2012; Gawne and Richmond 1993; Renart et al. 2010; A. S. Ecker et al. 2010). This dichotomy stems from viewing the system at two different scales; on a global scale, individual neurons seem to fire together producing large-scale oscillatory spiking patterns, on a more local scale, the firing activity of any two cortical neurons appear to be highly independent, suggesting a network which is more asynchronous. Because there is substantial evidence for both regimes, a full representation of cortical activity must incorporate and attempt to bridge the gap between these contrasting descriptions.

Recent work in sensory cortex (Okun et al. 2015) has attempted just this by utilizing 'population coupling', a quantity which relates the activity of an individual neuron to the summed spiking activity of the population in which the neuron is embedded. It was found that the population coupling of a neuron is a fixed quantity, dictated by the network/cell structure and therefore invariant to changes in external stimulus. The values of population coupling within primary visual cortex of awake mice exhibited a wide range and were distributed along a continuum suggesting possible functional differences in neurons with high- and low values of population coupling. This was indeed the case, neurons which displayed high values of population coupling were more active during application of external stimulus suggesting a larger role in coding of visual stimulus.

Here, we ask the question of whether these findings hold in primary motor cortex (M1). Specifically, are neurons with high values of population coupling within M1 most

responsible for commanding body movements or are there separate coding strategies for 'input' and 'output' regions within cortex?

Additionally, various neurological diseases which affect behavior are thought to be caused by an imbalance in cortical excitatory/inhibitory (E/I) signaling (Mccandless 2012; Nelson and Valakh 2015; Fagiolini and Leblanc 2011). Therefore, in an attempt to begin clarifying discrepancies between previous findings, we asked the question; what role does inhibitory signaling play within M1 in the context of population coupling?

To study this, we used 32-channel multielectrode arrays implanted in primary motor cortex of freely behaving rats (n=6) alongside an 8-camera infra-red motion capture system to take simultaneous neural and behavior recordings. We recorded the spiking activity of many single neurons simultaneously and measured precise 3-dimensional motion of the animals' bodies. For each neuron we recorded, our primary goal was to compare two properties: population coupling and body coupling. Population coupling (Okun et al. 2015) measures how similar the activity of an individual neuron is to the summed spiking activity of the population in which it is embedded. Body coupling measures how strongly the spiking of the neuron is related to body movement of the animal. We sought to determine whether neurons with high and low population coupling values had different body coupling values. Furthermore, in an attempt to increase the diversity in our data and relate to certain brain disorders, we pharmacologically manipulated (increased and decreased) $GABA_A$ signaling via intraperitoneal injection (global modulation, n=3) or cannula infusion (local M1 modulation, n=3).

A total of 1,684 spiking neurons were recorded (732 global, 952 local) across 257 total recordings (73 global, 184 local). Comparing across neurons, we found a large degree of variability in both population and body coupling values existed. These values seem to be distributed across respective continuous spectra as opposed more discrete intervals which agrees with previous findings (Okun et al. 2015) within other regions of cortex. We also found, by computing population coupling during periods of animal rest and movement independently,

that individual population coupling values were largely invariant to changes in behavior. This suggests population coupling is an effect of the network/cell structure and not a quantity which varies across relatively short time scales (<30 minutes). However, through altering inhibitory signaling, population coupling and subsequently body coupling for individual neurons can be tuned which suggests a causal relationship between population coupling and body coupling. Specifically, by increasing inhibition (both globally and locally), a marked increase (~10x) in values of population coupling across recorded neurons was seen as well as a corresponding increase in body coupling values, however the increase for body coupling was not as drastic (~2x).

Although our results show population coupling values are relatively fixed over shorter time scales, we did not determine whether population coupling remains constant across longer, day-to-day time scales. In order to determine this, single neurons across subsequent recordings and days within the same animal would need to be identified and tracked. Though this analysis is possible with the data contained here (specifically data recorded from animals with local changes in inhibition due to special MEA probe geometries), the question of long term population coupling fluctuations is beyond the scope of this thesis and is therefore reserved for future studies.

Our primary and most interesting result is that a significant trend exists across all rats and during all drug conditions wherein neurons with higher values of population coupling displayed lower values of body coupling (both STABS and MTASR) and vice versa (figures 24 & 25) This finding suggests that neurons whose activity is less correlated with that of the cortex may be most responsible for the coding of an organism's behavior. However, as population coupling is reduced to extremely low values, body coupling decreased significantly. This result suggests there may be a value or range of low population coupling which is optimal for the coding and commanding of body movements.

What repercussions do our results have regarding possible computational advantages/disadvantages within the decades-old synchronous vs. asynchronous cortical activity debate discussed in our introduction? It seems that motor cortex might make a compromise between these distinct modes of activity, optimizing the respective benefits while minimizing the drawbacks. The peaked nature observed when viewing BC vs. C_{pop} indicates that cortex reserves the process of behavior coding for those neurons which lie between these two extremes- i.e. neurons with highest values of body coupling exhibit low, but non-zero values of population coupling. This finding suggests motor cortex might make a trade-off between high information capacity (a characteristic of asynchronous networks) with the stronger signal throughput of synchronous networks. Recent work (Alkire, Hudetz, and Tononi 2008; Larremore, Shew, and Restrepo 2011; Hoang et al. 2013; Ollerenshaw et al. 2014; Clawson et al. 2017) has shown or hypothesized similar optimization strategies in other aspects of cortical function. Aside from these behavior-specific neurons, our results also indicate a large number of neurons which are highly involved with the activity of the network in which they are embedded. It may be that these neurons consolidate their activity in order to project more robust signals to distant regions of cortex. However, the actual function of these highly correlated neurons is still unclear and remains to be tested.

Comparing our results in motor cortex to previous findings on population coupling in visual cortex by Okun et al. reveals possible similarities and differences between sensory and motor areas of cortex. On one hand, our results strengthen the claim that population coupling is an effect of the network or cell structure as population coupling values computed during periods of rest versus periods of motion did not vary for individual neurons. If population coupling depends on network connectivity and is not a time-varying or region-specific quantity, this gives validity to its use as a more general analysis technique.

On the other hand, our findings seem to show separate and distinct coding strategies between different areas of cortex. Okun et al showed that in visual cortex (V1) neurons which

displayed higher values of population coupling were more active during periods of visual stimulus suggesting those neurons were more responsible for the coding of visual stimulus. Our results in motor cortex indicate that neurons whose activity are more coupled to the activity of the population are actually less coupled to the activity of the body and vice versa. These results suggest information for the execution of behavior is encoded by those neurons which are less coupled to the activity of the population in cortex. The difference in function-specific roles of neurons with high- and low population coupling values suggests separate and distinct input vs. output coding strategies within cerebral cortex.

Prior findings suggest the activity of cortex switches between more and less synchronized modalities: cortical activity is more asynchronous when the organism is actively engaged with the outside world (attention (Tan et al. 2014), wakefulness (Greenberg, Houweling, and Kerr 2008), motor planning (Poulet and Petersen 2008)) and more synchronous during periods of low environmental engagement (spontaneous activity (Poulet and Petersen 2008), sleep (Peyrache et al. 2012)). Our results suggest that these shifts in cortical synchrony could be due to changes in the balance of excitation and inhibition. For instance, the increases in inhibition we implemented in our experiments resulted in increased population coupling (i.e. increased synchrony.) However, a more important point from our findings is that if we only ask about the average population level synchrony, we may miss important differences in function across neurons. Averaging across neurons would miss the diversity of population coupling and the diversity in body coupling across neurons, and therefore would miss the functional differences that we observed between high and low population coupling neurons. On the time scale of one recording (30 min), we found that variability of population coupling across neurons was greater than variability over time, which suggests that understanding such variability across neurons is just as important as (perhaps more important than) understanding shifts in time.

While population coupling remains relatively constant within networks with fixed E/I ratios (on the time scale of our recordings), we have shown here that the coupling strength of

individual neurons to the network activity can be tuned by pharmacologically manipulating $GABA_A$ synaptic action. Relating this back to the initial motivation of the study, namely that autism spectrum disorder (ASD) is thought to be caused by an imbalance in the E/I ratio (Fagiolini and Leblanc 2011; Buckley and Holmes 2016) (whether ASD is an effect of too much excitation or inhibition is still heavily debated(Nelson and Valakh 2015)) as well as aberrant connectivity within and across certain regions of cortex (Noonan, Haist, and Müller 2009; Mizuno et al. 2006; C. Ecker et al. 2013). We see when inhibition is increased (both globally and locally) via muscimol application, a large increase in population coupling is observed (figures 24 & 25). When the activity of GABAergic neurons are disrupted (through application of pentylenetetrozol globally or bicuculline locally), population coupling values remain relatively unchanged from values obtained via no drug recordings. Future experiments utilizing genetically modified rat models of autism could shed light onto the specific direction of the E/I imbalance. If, for instance, autistic model rats were to display exceptionally high values of population/body coupling and these values could be driven down via a $GABA_A$ antagonist, this would add suggest an increase in inhibition within cortex. On the other hand, if population coupling values were on par with control groups and could be amplified via a $GABA_A$ agonist similar to muscimol, this would add further experimental evidence to the hypothesis that ASD is caused by a decrease in the E/I ratio.

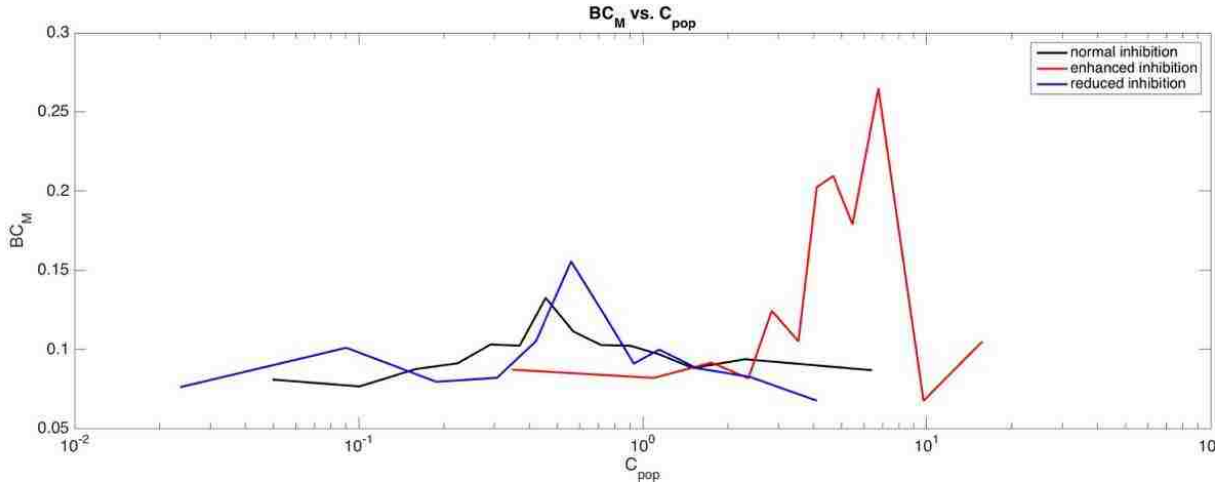

Figure 24– Body coupling (MTASR) vs. population coupling for normal, increased, and reduced inhibition. Lines represent binned average over many neurons. A significant increase in both population coupling and body coupling is seen with muscimol application. Bin sizes were chosen such that each bin contains an equal number of data points.

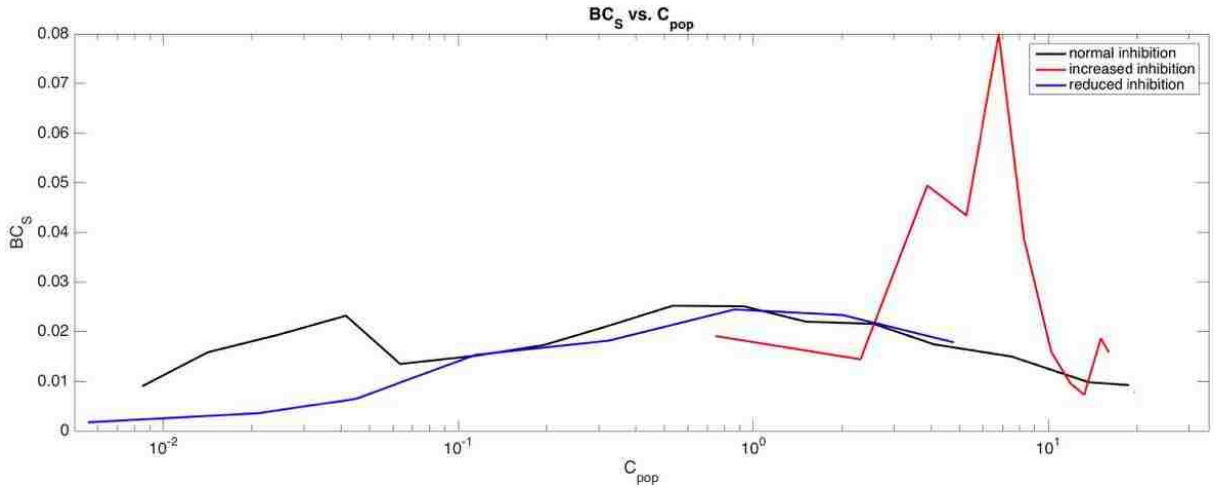

Figure 25 – Body coupling (STABS) vs. population coupling for normal, increased, and reduced inhibition. Lines represent binned average over many neurons. A significant increase in both population coupling and body coupling is seen with muscimol application. Bin sizes were chosen such that each bin contains an equal number of data points.

Bibliography

Alkire, Michael T, Anthony G Hudetz, and Giulio Tononi. 2008. “Consciousness and Anesthesia.” *Science (New York, N.Y.)* 322 (5903): 876–80. https://doi.org/10.1126/science.1149213.

Andersen, R A. 1997. “Multimodal Integration for the Representation of Space in the Posterior Parietal Cortex.” *Philosophical Transactions of the Royal Society of London. Series B, Biological Sciences* 352 (1360): 1421–28. https://doi.org/10.1098/rstb.1997.0128.

Averbeck, Bruno B., Peter E. Latham, and Alexandre Pouget. 2006. “Neural Correlations, Population Coding and Computation.” *Nature Reviews Neuroscience* 7 (5): 358–66. https://doi.org/10.1038/nrn1888.

Bader, Benjamin M, Anne Steder, Anders Bue Klein, Bente Frølund, Olaf H U Schroeder, and Anders A Jensen. 2017. *Functional Characterization of GABA A Receptor-Mediated Modulation of Cortical Neuron Network Activity in Microelectrode Array Recordings*. *Plos One* |. https://doi.org/10.1371/journal.pone.0186147.

Buckley, Ashura W., and Gregory L. Holmes. 2016. “Epilepsy and Autism.” *Cold Spring Harbor Perspectives in Medicine* 6 (4). https://doi.org/10.1101/cshperspect.a022749.

Canolty, R. T., K. Ganguly, S. W. Kennerley, C. F. Cadieu, K. Koepsell, J. D. Wallis, and J. M. Carmena. 2010. “Oscillatory Phase Coupling Coordinates Anatomically Dispersed Functional Cell Assemblies.” *Proceedings of the National Academy of Sciences* 107 (40): 17356–61. https://doi.org/10.1073/pnas.1008306107.

Clawson, Wesley P., Nathaniel C. Wright, Ralf Wessel, and Woodrow L. Shew. 2017. “Adaptation towards Scale-Free Dynamics Improves Cortical Stimulus Discrimination at the Cost of Reduced Detection.” Edited by Claus C. Hilgetag. *PLOS Computational Biology* 13 (5): e1005574. https://doi.org/10.1371/journal.pcbi.1005574.

Cohen, Marlene R., and Adam Kohn. 2011. “Measuring and Interpreting Neuronal Correlations.” *Nature Neuroscience* 14 (7): 811–19. https://doi.org/10.1038/nn.2842.

Dorn, J. D. 2002. “Estimating Membrane Voltage Correlations From Extracellular Spike Trains.” *Journal of Neurophysiology* 89 (4): 2271–78. https://doi.org/10.1152/jn.000889.2002.

Ecker, A S, P Berens, G A Keliris, M Bethge, N M Logothetis, and A S Tolias. 2010. “Decorrelated Neuronal Firing in Cortical Micro Circuits.” *Science* 327 (584): 584–87. https://doi.org/10.1126/science.1179867.

Ecker, C, L Ronan, Y Feng, E Daly, C Murphy, C E Ginestet, M Brammer, et al. 2013. “Intrinsic Gray-Matter Connectivity of the Brain in Adults with Autism Spectrum Disorder.” *Proc Natl Acad Sci U S A* 110 (32): 13222–27. https://doi.org/10.1073/pnas.1221880110.

Fagiolini, Michela, and Jocelyn J. Leblanc. 2011. “Autism: A Critical Period Disorder?” *Neural Plasticity*. https://doi.org/10.1155/2011/921680.

Gautam, Shree Hari, Thanh T. Hoang, Kylie McClanahan, Stephen K. Grady, and Woodrow L. Shew. 2015. “Maximizing Sensory Dynamic Range by Tuning the Cortical State to Criticality.” *PLoS Computational Biology* 11 (12): 1–15. https://doi.org/10.1371/journal.pcbi.1004576.

Gawne, T J, and B J Richmond. 1993. “How Independent Are the Messages Carried by Adjacent Inferior Temporal Cortical Neurons?” *The Journal of Neuroscience : The Official Journal of the Society for Neuroscience* 13 (7): 2758–71. https://doi.org/10.1523/jneurosci.0009-08.2008.

Georgopoulos, a P. 1996. “Arm Movements in Monkeys: Behavior and Neurophysiology.” *Journal of Comparative Physiology. A, Sensory, Neural, and Behavioral Physiology* 179 (5): 603–12. http://www.ncbi.nlm.nih.gov/pubmed/8888576.

Gray, C. M., and W. Singer. 1989. “Stimulus-Specific Neuronal Oscillations in Orientation Columns of Cat Visual Cortex.” *Proceedings of the National Academy of Sciences* 86 (5): 1698–1702. https://doi.org/10.1073/pnas.86.5.1698.

Greenberg, David S, Arthur R Houweling, and Jason N D Kerr. 2008. “Population Imaging of Ongoing Neuronal Activity in the Visual Cortex of Awake Rats.” *Nature Neuroscience* 11 (7): 749–51. https://doi.org/10.1038/nn.2140.

Hatsopoulos, N. G., C. L. Ojakangas, L. Paninski, and J. P. Donoghue. 1998. “Information about Movement Direction Obtained from Synchronous Activity of Motor Cortical Neurons.” *Proceedings of the National Academy of Sciences of the United States of America* 95 (26): 15706–11. https://doi.org/10.1073/pnas.95.26.15706.

Helias, Moritz, Tom Tetzlaff, and Markus Diesmann. 2014. “The Correlation Structure of Local Neuronal Networks Intrinsically Results from Recurrent Dynamics.” *PLoS Computational Biology* 10 (1). https://doi.org/10.1371/journal.pcbi.1003428.

Hoang, Thanh T., Stephen K. Grady, Shree Hari Gautam, and Woodrow L. Shew. 2013. “Inhibition, Sensory Dynamic Range, and Criticality in Barrel Cortex.” *2013 Neuroscience Meeting Planner* 71.20/OO12 (San Diego, CA): Online.

Illing, R B. 1996. “The Mosaic Architecture of the Superior Colliculus.” *Progress in Brain Research* 112: 17–34. https://doi.org/10.1016/S0079-6123(08)63318-X.

Kandel, E R, J H Schwartz, T M Jessell, Steven A Siegelbaum, and A.J. Hudspeth. 2014. *Principles of Neural Science, Fifth Edition*. *Neurology*. Vol. 3. https://doi.org/10.1036/0838577016.

Kolb, Bryan & Tees, Richard C. *The Cerebral Cortex of the Rat*. Cambridge: MIT Press, 1990.

La Rocha, Jaime De, Brent Doiron, Eric Shea-Brown, Krešimir Josić, and Alex Reyes. 2007. “Correlation between Neural Spike Trains Increases with Firing Rate.” *Nature* 448 (7155): 802–6. https://doi.org/10.1038/nature06028.

Larremore, Daniel B., Woodrow L. Shew, and Juan G. Restrepo. 2011. “Predicting Criticality and Dynamic Range in Complex Networks: Effects of Topology.” *Physical Review Letters* 106 (5): 1–4. https://doi.org/10.1103/PhysRevLett.106.058101.

Matsumura, M, T Sawaguchi, T Oishi, K Ueki, and K Kubota. 1991. “Behavioral Deficits Induced by Local Injection of Bicuculline and Muscimol into the Primate Motor and Premotor Cortex.” *Journal of Neurophysiology* 65 (6): 1542–53.

Markopoulos, Foivos, Dan Rokni, David H. Gire, and Venkatesh N. Murthy. 2012. “Functional Properties of Cortical Feedback Projections to the Olfactory Bulb.” *Neuron* 76 (6): 1175–88. https://doi.org/10.1016/j.neuron.2012.10.028.

Maynard, E M, N G Hatsopoulos, C L Ojakangas, B D Acuna, J N Sanes, R a Normann, and J P Donoghue. 1999. “Neuronal Interactions Improve Cortical Population Coding of Movement Direction.” *The Journal of Neuroscience : The Official Journal of the Society for Neuroscience* 19 (18): 8083–93. https://doi.org/http://www.jneurosci.org/cgi/content/full/19/18/8083;http://www.jneurosci.org/cgi/content/abstract/19/18/8083.

Mccandless, D W. 2012. “Epilepsy and Autism,” 1–18. https://doi.org/10.1007/978-1-4614-0361-6.

Mizuno, Akiko, Michele E. Villalobos, Molly M. Davies, Branelle C. Dahl, and Ralph Axel Müller. 2006. “Partially Enhanced Thalamocortical Functional Connectivity in Autism.” *Brain Research* 1104 (1): 160–74. https://doi.org/10.1016/j.brainres.2006.05.064.

Murthy, V N, E E Fetz, N Murthy, and Eberhard E Fetz. 2013. “Synchronization of Neurons during Local Field Potential Oscillations in Sensorimotor Cortex of Awake Monkeys Synchronization of Neurons During Local Field Potential Oscillations in Sensorimotor Cortex of Awake Monkeys” 76 (6): 3968–82.

Nelson, Sacha B., and Vera Valakh. 2015. “Excitatory/Inhibitory Balance and Circuit Homeostasis in Autism Spectrum Disorders.” *Neuron*. https://doi.org/10.1016/j.neuron.2015.07.033.

Nelson, Sacha B., and Vera Valakh. 2015. “Excitatory/Inhibitory Balance and Circuit Homeostasis in Autism Spectrum Disorders.” *Neuron*. https://doi.org/10.1016/j.neuron.2015.07.033.

Noonan, Sarah K., Frank Haist, and Ralph Axel Müller. 2009. “Aberrant Functional Connectivity in Autism: Evidence from Low-Frequency BOLD Signal Fluctuations.” *Brain Research* 1262: 48–63. https://doi.org/10.1016/j.brainres.2008.12.076.

O’Keefe, John, and Michael L. Recce. 1993. “Phase Relationship between Hippocampal Place Units and the EEG Theta Rhythm.” *Hippocampus* 3 (3): 317–30. https://doi.org/10.1002/hipo.450030307.

Okun, Michael, Nicholas A. Steinmetz, Lee Cossell, M. Florencia Iacaruso, Ho Ko, Péter Barthó, Tirin Moore, et al. 2015. “Diverse Coupling of Neurons to Populations in Sensory Cortex.” *Nature* 521 (7553): 511–15. https://doi.org/10.1038/nature14273.

Ollerenshaw, Douglas R., He J V Zheng, Daniel C. Millard, Qi Wang, and Garrett B. Stanley. 2014. “The Adaptive Trade-off between Detection and Discrimination in Cortical Representations and Behavior.” *Neuron* 81 (5). Elsevier Inc.: 1152–64. https://doi.org/10.1016/j.neuron.2014.01.025.

Pernice, Volker, Benjamin Staude, Stefano Cardanobile, and Stefan Rotter. 2011. “How Structure Determines Correlations in Neuronal Networks.” *PLoS Computational Biology* 7 (5). https://doi.org/10.1371/journal.pcbi.1002059.

Peyrache, Adrien, Nima Dehghani, Emad N Eskandar, Joseph R Madsen, William S Anderson, Jacob A Donoghue, Leigh R Hochberg, Eric Halgren, Sydney S Cash, and Alain Destexhe. 2012. “Spatiotemporal Dynamics of Neocortical Excitation and Inhibition during Human Sleep.” *Proceedings of the National Academy of Sciences of the United States of America* 109 (5): 1731–36. https://doi.org/10.1073/pnas.1109895109.

Poulet, J. F A, and C. C H Petersen. 2008. “Internal Brain State Regulates Membrane Potential Synchrony in Barrel Cortex of Behaving Mice.” *Nature* 454 (7206): 881–85. https://doi.org/10.1038/nature07150.

Renart, Alfonso, Jaime De Rocha, Peter Bartho, Liad Hollender, Alex Reyes, and Kenneth D Harris. 2010. “The Asynchronus State in Cortical Circuits.” *Science* 327 (5965): 587–90. https://doi.org/10.1126/science.1179850.The.

Riehle, Alexa, Sonja Gru, Markus Diesmann, and Ad Aertsen. 2009. “Spike Synchronization and Rate Modulation Differentially Involved in Motor Cortical Function Spike Synchronization and Rate Modulation Differentially Involved in Motor Cortical Function Lations among Neurons with High Temporal.” *Science* 1950 (1997): 1950–53. https://doi.org/10.1126/science.278.5345.1950.

Rolls, Edmund T., Alessandro Treves, and Martin J. Tovee. 1997. “The Representational Capacity of the Distributed Encoding of Information Provided by Populations of Neurons in Primate Temporal Visual Cortex.” *Experimental Brain Research* 114 (1): 149–62. https://doi.org/10.1007/PL00005615.

Rossant, Cyrille, Shabnam N Kadir, Dan F M Goodman, John Schulman, Maximilian L D Hunter, Aman B Saleem, Andres Grosmark, et al. 2016. “Spike Sorting for Large, Dense Electrode Arrays.” *Nature Neuroscience* 19 (March). Nature Publishing Group, a division of Macmillan Publishers Limited. All Rights Reserved.: 634. http://dx.doi.org/10.1038/nn.4268.

Salinas, Emilio, and Terrence J. Sejnowski. 2001. “Correlated Neuronal Activity and the Flow of Neural Information.” *Nature Reviews Neuroscience* 2 (8): 539–50. https://doi.org/10.1038/35086012.

Schneidman, Elad, William Bialek, and Michael J Berry. 2003. “Synergy, Redundancy, and Independence in Population Codes. TL - 23.” *The Journal of Neuroscience : The Official Journal of the Society for Neuroscience* 23 VN-r (37): 11539–53. http://www.ncbi.nlm.nih.gov/pubmed/14684857.

Shew, W. L., H. Yang, S. Yu, R. Roy, and D. Plenz. 2011. “Information Capacity and Transmission Are Maximized in Balanced Cortical Networks with Neuronal Avalanches.” *Journal of Neuroscience* 31 (1): 55–63. https://doi.org/10.1523/JNEUROSCI.4637-10.2011.

Sitdikova, Guzel, Andrei Zakharov, Sona Janackova, Elena Gerasimova, Julia Lebedeva, Ana R. Inacio, Dilyara Zaynutdinova, Marat Minlebaev, Gregory L. Holmes, and Roustem Khazipov. 2014. “Isoflurane Suppresses Early Cortical Activity.” *Annals of Clinical and Translational Neurology* 1 (1): 15–26. https://doi.org/10.1002/acn3.16.

Stein, Barry E, Terrence R Stanford, and Benjamin A Rowland. 2009. “The Neural Basis of Multisensory Integration in the Midbrain: Its Organisation and Maturation.” *Hearing Research* 258: 4–15. https://doi.org/10.1016/j.heares.2009.03.012.The.

Tan, Andrew Y Y, Yuzhi Chen, Benjamin Scholl, Eyal Seidemann, and Nicholas J. Priebe. 2014. “Sensory Stimulation Shifts Visual Cortex from Synchronous to Asynchronous States.” *Nature* 509 (7499): 226–29. https://doi.org/10.1038/nature13159.

Uhlhaas, P J, G Pipa, B Lima, L Melloni, S Neuenschwander, D Nikolic, and W Singer. 2009. “Neural Synchrony in Cortical Networks: History, Concept and Current Status.” *Front Integr Neurosci* 3: 17. https://doi.org/10.3389/neuro.07.017.2009.

Womelsdorf, Thilo, Jan Mathijs Schoffelen, Robert Oostenveld, Wolf Singer, Robert Desimone, Andreas K. Engel, and Pascal Fries. 2007. “Modulation of Neuronal Interactions through Neuronal Synchronization.” *Science* 316 (5831): 1609–12. https://doi.org/10.1126/science.1139597.

Zohary, Ehud, Michael N. Shadlen, and William T. Newsome. 1994. “Correlated Neuronal Discharge Rate and Its Implications for Psychophysical Performance.” *Nature* 370 (6485): 140–43. https://doi.org/10.1038/370140a0.

Appendices

Sample .prb file

```
channel_groups = {
   # Shank index.
   0:
      {
         # List of channels to keep for spike detection.
         'channels': [12, 4, 5, 13, 2, 7, 3, 6, 8, 1, 9, 0, 15, 14, 11, 10, 16, 17, 20, 21, 18, 30, 29,
31, 28, 19, 27, 25, 22, 24, 23, 26],

         # Adjacency graph.
         'graph': [

            (12, 4), (12, 2),
            (4, 2), (4, 7), (4, 5),
            (5, 7), (5, 3), (5, 13),
            (13, 3), (13, 6),
                                 (6, 3),
                                 (3, 7),
            (7, 2),
                                 (8, 1), (8, 15),
            (1, 15), (1, 14), (1, 9),
            (9, 14), (9, 11), (9, 0),
                                 (0, 11), (0, 10),
                                 (10, 11),
                                 (11, 14),
                                 (14, 15),
                                 (16, 17), (16, 18),
            (17, 18), (17, 30), (17, 20),
            (20, 30), (20, 29), (20, 21),
            (21, 29), (21, 31),
            (31, 29),
                                 (29, 30),
                                 (30, 18),
                                 (28, 19), (28, 22),
            (19, 22), (19, 24), (19, 27),
            (27, 24), (27, 23), (27, 25),
            (25, 23), (25, 26),
                                 (26, 23),
                                 (23, 24),
                                 (24, 22),
         ],

         # 2D positions of the channels,
         'geometry': {
                           12: (-1, 7),
                                 4: (-1, 5),
                                 5: (-1, 3),
                                 13: (-1, 1),
```

```
                2: (1, 6),
                7: (1, 4),
                3: (1, 2),
                6: (0, 0),
                8: (9, 7),
                1: (9, 5),
                9: (9, 3),
                0: (9, 1),
                15: (11, 6),
                14: (11, 4),
                11: (11, 2),
                10: (10, 0),
                16: (19, 7),
                17: (19, 5),
                20: (19, 3),
                21: (19, 1),
                18: (21, 6),
                30: (21, 4),
                29: (21, 2),
                31: (20, 0),
                28: (29, 7),
                19: (29, 5),
                27: (29, 3),
                25: (29, 1),
                22: (31, 6),
                24: (31, 4),
                23: (31, 2),
                26: (30, 0),

        }
    }

}
```

Sample .prm file

```
##########################
# SpikeDetekt parameters #
##########################

experiment_name = 'nodrug'
raw_data_files = experiment_name + '.dat'
prb_file = 'aPC_buzsaki_1shank_090915_c.prb'
nbits = 16
voltage_gain = 1.

sample_rate = 30000
nchannels = 32


# Filtering
# ---------
filter_low = 250. # Low pass frequency (Hz)
filter_high = 5000. # 0.95 * .5 * sample_rate
filter_butter_order = 3  # Order of Butterworth filter.

filter_lfp_low = 0  # LFP filter low-pass frequency
filter_lfp_high = 300  # LFP filter high-pass frequency


# Chunks
# ------
chunk_size = int(1. * sample_rate)  # 1 second
chunk_overlap = int(.015 * sample_rate)  # 15 ms

# Spike detection
# ---------------
# Uniformly scattered chunks, for computing the threshold from the std of the
# signal across the whole recording.
nexcerpts = 50
excerpt_size = int(1. * sample_rate)
threshold_strong_std_factor = 9.
threshold_weak_std_factor = 4.
detect_spikes = 'negative'
#precomputed_threshold = None

# Connected component
# -------------------
```

```
connected_component_join_size = int(.00005 * sample_rate)

# Spike extraction
# ----------------
extract_s_before = 24
extract_s_after = 36
waveforms_nsamples = extract_s_before + extract_s_after

# Features
# --------
nfeatures_per_channel = 3  # Number of features per channel.
pca_nwaveforms_max = 10000


##########################
# KlustaKwik parameters #
##########################
MaskStarts = 100
#MinClusters = 100
#MaxClusters = 110
MaxPossibleClusters =  500
FullStepEvery =  10
MaxIter = 10000
RandomSeed =  654
Debug = 0
SplitFirst = 20
SplitEvery = 100
PenaltyK = 0
PenaltyKLogN = 1
```

Animal protocols

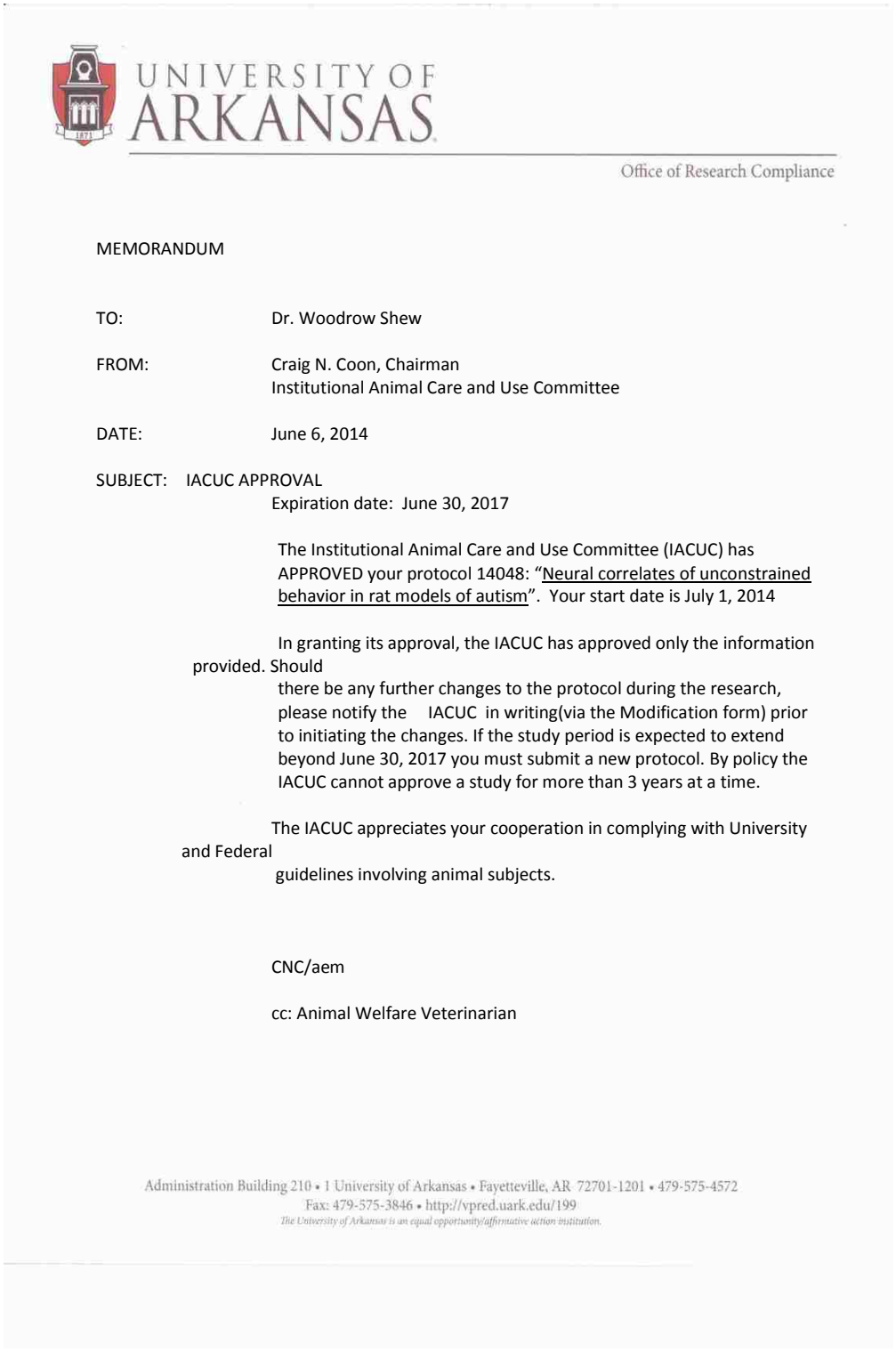

UNIVERSITY OF ARKANSAS

Office of Research Compliance

MEMORANDUM

TO: Dr. Woodrow Shew

FROM: Craig N. Coon, Chairman
Institutional Animal Care and Use Committee

DATE: June 6, 2014

SUBJECT: IACUC APPROVAL
Expiration date: June 30, 2017

The Institutional Animal Care and Use Committee (IACUC) has APPROVED your protocol 14048: "Neural correlates of unconstrained behavior in rat models of autism". Your start date is July 1, 2014

In granting its approval, the IACUC has approved only the information provided. Should there be any further changes to the protocol during the research, please notify the IACUC in writing(via the Modification form) prior to initiating the changes. If the study period is expected to extend beyond June 30, 2017 you must submit a new protocol. By policy the IACUC cannot approve a study for more than 3 years at a time.

The IACUC appreciates your cooperation in complying with University and Federal guidelines involving animal subjects.

CNC/aem

cc: Animal Welfare Veterinarian

Administration Building 210 • 1 University of Arkansas • Fayetteville, AR 72701-1201 • 479-575-4572
Fax: 479-575-3846 • http://vpred.uark.edu/199
The University of Arkansas is an equal opportunity/affirmative action institution.

UNIVERSITY OF ARKANSAS

Research Compliance
Office of the Director

MEMORANDUM

TO: Woodrow Shew

FROM: Craig N. Coon, Chairman
Institutional Animal Care
And Use Committee

DATE: July 2, 2012

SUBJECT: IACUC PROTOCOL **APPROVAL**
Expiration date : **December 31, 2012**

The Institutional Animal Care and Use Committee (IACUC) has **APPROVED** Protocol **#12054- "PILOT STUDY: QUANTIFYING THE BEHAVIORAL REPERTORIES OF NORMAL AND VALPROIC (VPA) RATS**". You may begin this study immediately.

The IACUC encourages you to make sure that you are also in compliance with other UAF committees such as Biosafety, Toxic Substances and/or Radiation Safety if your project has components that fall under their purview.

In granting its approval, the IACUC has approved only the protocol provided. Should there be any changes in the protocol during the research, please notify the IACUC in writing [Modification Request form] **prior** to initiating the changes. If the study period is expected to extend beyond **12-31-2012,** you may request an extension [Modification Request form] up to 06-28-2015, which is 3 years from the original approval date. By policy the IACUC cannot approve a study for more than 3 years at a time.

The IACUC appreciates your cooperation in complying with University and Federal guidelines for research involving animal subjects.

cnc/car

cc: Animal Welfare Veterinarian

120 Ozark Hall • University of Arkansas • Fayetteville, AR 72701
Voice (479) 575-3845 • Fax (479) 575-3846